Synthesis, characterizations, crystal structure, inhibition effects and theoretical study of novel Schiff base on the corrosion of carbon steel in 1 M HCl

Soraya Boukazoula, Djahida Haffar, Riadh Bourzami, Linda Toukal, Vincent Dorcet

HIGHLIGHTS

- Synthesis of new Schiff base ligand the 2,4- Bis (2-hydroxy naphthaldehyde) diiminotholuene.
- Characterization of ligand by 1HNMR, 13CNMR, IR, UV-Vis.
- The structure of ligand was determined by X-ray diffraction method.
- The system carbone steel / HCl was studied using chemical (weight loss) and electrochemical (impedance spectroscopy and potentiodynamic) measurements
- The synthesized compound follow a physisorption-chemisorption mechanism process.
- SEM studies of metal surfaces confirmed the formation of the adsorbed layer of inhibitor.
- Theoretical studies using DFT calculations.

Synthesis, characterizations, crystal structures, inhibition effects and theoretical study of novel Schiff base derived from hydroxynaphthaldehyde on the corrosion of carbon steel in 1 M HCl

Soraya Boukazoula[a], Djahida Haffar[a], Riadh Bourzami[b], Linda Toukal[a]*, Vincent Dorcet[c]

[a]*Laboratory of Electrochemistry and Materials (LEM) Department of Engineering Process, Faculty of Technology, Ferhat Abbas University Setif-1, Setif 19000, Algeria.*
[b]*Emerging Materials Reaserch Unit, Ferhat Abbas University Setif-1, Setif 19000, Algeria.*
[c]*Univ Rennes, CNRS, ISCR (Institut des Sciences Chimiques de Rennes) - UMR 6226, 35000 Rennes, France.*

Abstract

A novel Schiff base 2, 4- Bis (2-hydroxy naphthaldehyde) diiminotholuene (L), was prepared and characterized by the analysis techniques: FT-IR, UV-Vis, ^{1}H and ^{13}C NMR. X-Ray Diffraction (XRD), showing that the L was crystallized in phenol-imine form. The corrosion inhibition of carbon steel in 1 M hydrochloric acid solutions of ligand L was studied using chemical (weight loss) and electrochemical (potentiodynamic and electrochemical impedance spectroscopy (EIS)) measurements, these measurements show that the inhibition efficiency obtained by this compound increased by increasing the concentration of L. The polarization studies show that this L acts as mixed type inhibitor. This inhibitor functions through adsorption following Langmuir isotherm. The UV-Vis absorption spectroscopy was used to investigate the forming of complex between inhibitor L and Fe. The scanning electron microscopy (SEM) studies the metal surfaces confirming the formation of the adsorbed layer of inhibitor, which slows down the corrosion process in the corrosive solution. The Density functional theory (DFT) and Simulations of the Molecular Dynamics (SMD) were used to determine the relationship between quantum chemical parameters and their inhibition efficiencies, and the correlation between theoretical and experimental results was discussed.

Keywords: Synthesis, Schiff base, XRD, Corrosion, Acid inhibition, DFT.

1. Introduction

Organic compounds have been studied with great interest for corrosion inhibition. Which the corrosion of mild steel in acid solutions can be readily inhibited by the use of chemical inhibitors [1].

Compounds containing an azomethine group (-CH=N-) are known as Schiff bases. They are usually formed by condensation of a primary amine with a carbonyl compound [2].

The applicability of aromatic Schiff bases compounds as corrosion inhibitors for metals in acidic media has been recognized for a long time [3].

Organic compounds containing heteroatom like nitrogen, phosphorus, oxygen, sulfur, as well as aromatic rings, present free electron pairs and the presence of -CH=N- group in their molecular structure can facilitate their adsorption on the metal surfaces [4-8].

Some Schiff base compounds have been studied which have shown good inhibition efficiency, for metals and alloys against acidic media, this inhibitors function through adsorption on metal surface blocking the active sites by displacing water molecules and forming a compact barrier film to decrease corrosion rate [9].

This adsorption process depends primarily on the nature of the metal and the surface charge, the chemical structure of the corrosion inhibitor, the type of corrosive electrolyte, and the temperature of the corrosion reaction [10].

Recently, there has been a substantial effort in the literature in particular on the use of Density Functional Theory (DFT) as a theoretical method in the modelization of inhibitor / surface interaction [11, 12], moreover, the use of quantum chemical calculations is very important in establishing the correlation between molecular structure and chemical reactivity of corrosion inhibition process.

Mild steel is widely used in many industries due to its mechanical properties and low cost [13]. They undergo corrosion with time this is due to attack by acid or basic solutions used in pickling. For achieve higher life time of the mild steel, corrosion inhibitors are needed for lower iron dissolution [14].

The aim of this article is the synthesis and the characterization of a new compound Schiff base 2,4- Bis (2-hydroxy naphthaldehyde) diiminotholuene and the investigation of its behavior as new inhibitor for the corrosion of carbon steel against 1 M HCl solution. The structure of the Schiff base was determined via X-ray diffraction analysis, ^{1}H NMR, ^{13}C NMR, FT-IR and UV-Vis. Inhibitive action of Schiff base on corrosion of Carbon steel in 1 M HCl was investigated through weigh loss measurements (gravimetry), polarization curves and electrochemical impedance spectroscopy. The effect of temperature on inhibition efficiency was studied, and through it, the adsorption mechanism on metal surface was discussed, the correlation between the theoretical results by using the density functional theory and the results experimental inhibition efficiencies of this inhibitor was invertigated.

The surface morphology of steel was analyzed by scanning electron microscopy (SEM) in order to confirm the inhibitory action of Schiff base ligand.

2. Experimental

2.1. Materials and physic-chemical measurements

The chemical products used for the synthesis and corrosion studies are of analytical grade. 2.4-diaminotholuene, 2-hydroxy naphthaldehyde and solvents were purchased from Sigma-Aldrich and used without further purification. The UV-Visible spectrum was recorded in DMF between 200 and 800 nm using JASCO Ve 650 spectrophotometer with quartz cells of 1 cm path length. ^{1}H-NMR and ^{13}C-NMR spectra were recorded at 25 °C on Bruker Avance DPX250 spectrometer with the working frequency of 250 MHz. IR spectrum was obtained by using KBr pellets in 500-4000 cm^{-1} range, by using FT/IR-JASCO 4200 instrument.

2.2. Synthesis of new Schiff base 2,4- Bis (2-hydroxy naphthaldehyde) diiminotholuene

Schiff base 2,4- Bis (2-hydroxy naphthaldehyde) diiminotholuene was synthesized by condensation of methanolic solutions of 2.4-diaminotholuene (1.22 g, 10 mmol) and 2-hydroxy naphthaldehyde (3.44 g, 20 mmol) taken in a molar ratio of 1:2 (Scheme 1). The mixture was stirred at 60 °C for 3 h under a nitrogen atmosphere. The yellow precipitate was isolated by filtration washed with methanol, diethylether and dried in vacuum [5, 15].

The product was recrystallized in dichloromethane/methanol (1/1) and dried at room temperature. The final product was recovered with yield: 87%; M.p: 222°C; IR (KBr, cm^{-1}): 3450 υ (OH), 2921-3053 υ (CH), 1624, 1605 υ (HC=N), 1318 υ (C=C), 1247 υ (C-O), 1082 δ (O-H); UV-Vis (λ (nm), DMF as solvent): 263.17, 319, 393.12, 443.90 and 466.96 nm; ^{1}H-NMR (400 MHz, DMSO-d6, (δ) ppm): 15.80,16 (2s, 2H, -O<u>H</u>), 9.74,9.79 (2s, 2H, C<u>H</u>=N), 7.02-8.58 (m, aromatic protons); 2.51 (s, 3H, -C<u>H</u>$_3$); ^{13}C-NMR (100 MHz; DMSO-d6, (δ) ppm): 171.24, 172.30 (-<u>C</u>H=N-); 17.92 (-<u>C</u>H$_3$); 108.97 to 156.00 (aromatic carbons); 155.73, 156 (-<u>C</u>-OH).

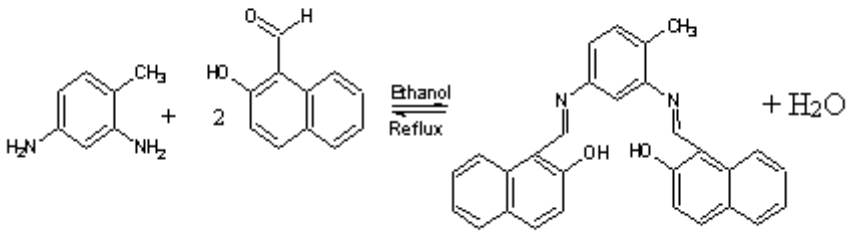

Scheme 1. Reaction scheme for the synthesis of Schiff base 2,4- Bis (2-hydroxynaphthaldehyde) diiminotholuene.

2.3. X-Ray Diffraction

Orange single crystal of the synthesized Schiff base ligand was obtained using the method of the diffusion of CH_4 into MeOH solution at room temperature. The diffraction data on single crystal of the dimensions (0.21 × 0.18 × 0.16 mm) mm^3 were collected at 150 K on a Bruker D8-Venture-photon diffractometer, equipped with graphite-monochromated Mo/Ka radiation (λ=0.71073 Å). Transmission factors: Tmin/Tmaxwas about 0.786/0.987. The structure was solved by direct methods by using SHELXL-2015 and SHELXL- 2017 programs (Sheldrick, 2015 and Sheldrick, 2017) [16] and refined on F2 by the full-matrix least-squares methods, the nonhydrogen atoms were subjected to anisotropic refinement and the hydrogen atoms were included in geometric positions but not refined.

2.4. Quantum chemical calculations

To investigate the effect of molecular structure on the inhibition mechanism and inhibition efficiency, some quantum calculations were performed [17], by using Gaussian software version 9.0 [18]. All the calculations were performed with complete geometry optimization using the hybrid B3LYP functional level with a higher basis set denoted by 6-31G (d, p) [19-21]. Some quantum chemical parameters were calculated through the values of the energies of the HOMO and LUMO using the following formulas [22]:

Ionization Energy (I)	$I = -E_{HOMO}$	(1)
Electron Affinity (A)	$A = -E_{LUMO}$	(2)
ΔE_{GAP} (eV)	$\Delta E_{GAP} = E_{LUMO} - E_{HOMO}$	(3)
Chemical Hardness (η)	$\eta = (E_{LUMO} - E_{HOMO})/2$	(4)
Chemical Softness (σ)	$\sigma = 1/\eta$	(5)
Electrophilicity Index (ω)	$\omega = \mu^2/2\,\eta$	(6)
Electronegativity (χ)	$\chi = (I + A)/2$	(7)
Chemical Potential (μ)	$\mu = -\chi$	(8)

2.5. Solutions

The aggressive solutions of 1 M HCl was prepared by dilution of HCl by distilled water. Otherwise, the inhibitor solutions of Schiff base ligand L were prepared in 1M HCl to which DMF was added for solubility reasons. The corrosion tests were performed in solution in the

absence and presence of various concentrations (5.10^{-5}, 10^{-4}, 5.10^{-4}, 10^{-3}, 5.10^{-3} M) of Schiff base ligand L.

2.6. Gravimetric measurement

The study of the concentration effect on the corrosion inhibitive activity of the tested ligand was studied exploiting weight loss measurements. The carbon steel X48 samples were polished with emery paper and degreased with acetone. The carbon steel samples are cylindrical in shape with an area equal to 1.5 cm^2.

Specimens were immersed in an inclined position, in 50 ml 1 M HCl solution for 24 h at room temperature (25 °C) in absence and presence of various concentrations of the synthesized ligand L. The weight of the specimens before and after immersion was determined using an analytical balance of 0.0001 mg accuracy. Experiments were carried out in triplicate and the average of the triplicate values was used.

2.7. Electrochemical measurements

Electrochemical Impedance Spectroscopy (EIS) and Potentiodynamic polarization experiments were carried out using a Gamry Potentiostat (Reference 3000) integrated with Gamry Echem Anayst software a conventional electrolytic cell three-electrode arrangement, the working electrode is a Carbon steel of 0.19 cm^2 surface disc-like with the following composition: C 0.52-0.50 %, Mn 0.5-0.80 %, Si 0.40 %, P 0.035%, S ≤ 0.035% and the remaining amount is Fe. The working surface was ground for abrasive papers, degreased by distilled water and washed with acetone and finally dried with Josef paper. The auxiliary electrode was a graphite bar and the reference was Ag/AgCl electrode. Before starting, Open Circuit Potential (OCP) was maintained for 30 minutes until it reaches a steady state. All experiments were conducted at 25°C. In addition, potentiodynamic polarization curves were determined after establishing of the open circuit potential with scan rate of 0.5 mV s^{-1}.

The Electrochemical Impedance measurements (EIS) were performed at Open Circuit Potential (OCP) in the frequency range of 100 kHz to 10 mHz with 10 points per decade.

3. Results and discussion

3.1. XRD analysis

The single crystal X-ray diffraction study revealed that the molecular formula of the ligand L was $C_{29}H_{22}N_2O_2$, the crystal data, data collection and structure refinement parameters L are given in the Table 1. The asymmetric unit of ligand L provided with the atom numbering is given in the Figure 1a, and the Table 2 collects some selected angles measurements and bonds

lengths characteristic of the ligand L. The C-C and C=C bonds lengths characteristic of the aromatic rings are between 1.429 and 1.351 Å and all its angles measurements are in the range [119.6-121.8°], which is consistent with the sp^2 hybridization of all carbon atoms, otherwise, the C12-N1 and C16-N2 bond lengths are 1.416 (4) Å and 1.420 (4) Å respectively, they are compatible with the single bond C-N which are longer than the imine function C=N (C11=N1 and C19=N2 are 1.304 (5) Å, 1.279 (4) Å respectively) [23]; these values are in the same order compared to the corresponding lengths (C-N) 1.4171(18) and (C=N) 1.2794(18) Å of (E)-4-nitro-2-[(o-tolylimino)methyl]phenol (L) [24-26], similarly, the bond length C1-O1 is 1.302(4) Å and the C29-O2 is 1.339(4) Å are also consistent with the O–C single bond [27, 28]. All other angles measurements and bonds lengths are in normal norm and are in good agreement with those reported in similar Schiff base ligand [26]. In addition, the crystallographic data for the structure reported in this paper has been deposited in the Cambridge Crystallographic Center (CCDC), with CCDC number 2016676.

Table 1
Crystal data, data collection and structure refinement parameters for the ligand L.

Molecular formula	$C_{29}H_{22}N_2O_2$
Molecular weight (g/mol)	430.48
Temperature (K)	150
Mo-Kα radiation, λ	0.71073 Å
Crystal system	Orthorhombic
Space group	$Pna2_1$
a (Å)	19.1041 (16)
b (Å)	20.0742 (14)
c (Å)	5.6083 (5)
Volume ($Å^3$)	2150.8 (3)
Z	4
Crystal dimension	0.21 × 0.18 × 0.16 mm
Crystal /color	Orange
D_x (mg m^{-3})	1.329
μ (mm^{-1})	0.08
F (000)	904
Refinement method	Full-matrix least-squares
Data/restraints/parameters	5569 /1/309
Range/indices (h, k, l)	-22,24; -26,25; -7,7
θ_{max} , θ_{min}	27.5°, 2.9°
measured reflections	11986
independent reflections	4807
Reflections with I > 2σ(I)	3823
S Goodness of fit on F^2	1.05
$\Delta\rho_{max}$, $\Delta\rho_{min}$ (e $Å^{-3}$)	0.16, - 0.21
R[F^2 > 2σ(F^2)]	0.048
wR(F^2)	0.108

Table 2
Experimental selected bond lengths (Å) and angle measurements (°) of the ligand L.

Bond lengths (Å)	valeurs Experimental	Bond angles (°)	valeurs Experimental
C29-O2	1.339(4)	O1-C1-C2	118.9(3)
C1-O1	1.302(4)	O1-C1-C10	122.1(3)
C11-N1	1.304(5)	C1-O1-H10	108.0(3)
C12-N1	1.416(4)	N1-C11-C10	123.2(3)
C19-N2	1.279(4)	C17-C12- N1	117.4(2)
C16-N2	1.420(4)	C13-C12-N1	123.0(3)
O1-H10	0.83 (11)	C11-N1-C12	123.8(2)
O2-H2A	0.8400	O2-C29-C28	116.4(3)
		O2-C29-C20	122.5(3)
		C29-O2-H2A	109.5
		C19-N2-C16	120.8(2)
		N2-C19-C20	121.1(3)
		C2-C1-C10	119.1(3)
		C3-C2-C1	120.7(3)
		C13-C12-C17	119.6(3)
		C13-C14-C15	121.8(3)

Moreover, the two hydroxyl groups are involved in intramolecular of the type O—H···N hydrogen bonds, the proton transfer from the hydroxyl oxygen atom of the parent aromatic aldehyde to the nitrogen atom requests a small amount of energy, this proton transfer causes a conformation changes of the molecular structure of ligand L, especially in the π-electron distribution [29], in this way, the asymmetric unit of L (Figure 1b) is far from a planar geometry, the two binaphthaldehyde moieties and the benzene moiety belong to three different plans, where the angles between the plans are 7.06, 61.68 and 61.90°. The Table 3 collects the intramolecular hydrogen bonds with corresponding characteristic donors and acceptors angles and bond lengths.

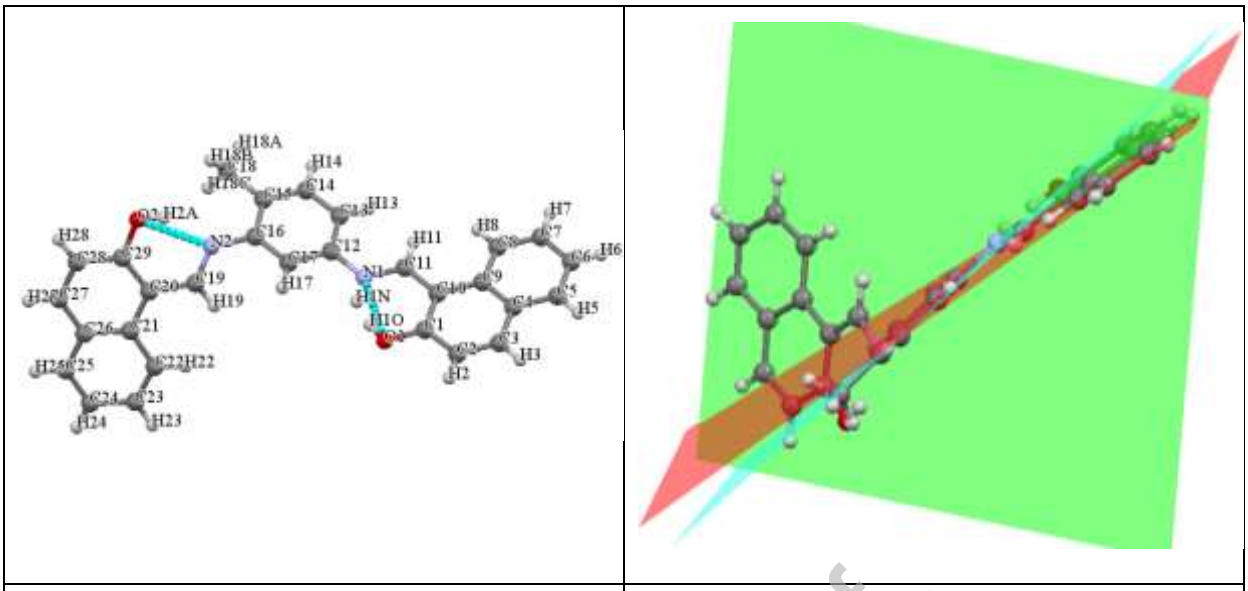

(a) (b)

Figure 1. Asymmetric unit of the compound L (a) provided with intramolecular hydrogen bonds and atomic numbering (b) provided with geometric carrier plans.

Table 3
Hydrogen-bond geometry (Å, °).

D—H···*A*	D—H	H···A	D···A	D—H···A
C2—H2···O1^{i}	0.95	2.56	3.368(4)	143
C28—H28···O2^{ii}	0.95	2.49	3.292(4)	143

Symmetry code: (i) −*x*+1, −*y*+1, *z*+1/2; (ii) −*x*, −*y*+1, *z*−1/2.

Furthermore, the ligand L crystallizes in orthorhombic lattice with space group $Pna2_1$, where the unit cell parameters are a = 19.1041 (16) Å, b = 20.0742 (14) Å, c = 5.6083 (5) Å and a filling rate is four molecules per unit cell Z = 4 (Figure 2), which the density is d = 1.329 g.cm^{-3}, furthermore, the unit cell is characterized by (x y z) identity, two glide planes perpendicular to the direction [0 1 0] with glide component [½ 0 0] and finally 2-fold screw axis with the direction [0 0 1] at the points (0 0 z) with screw component [0 0 ½].

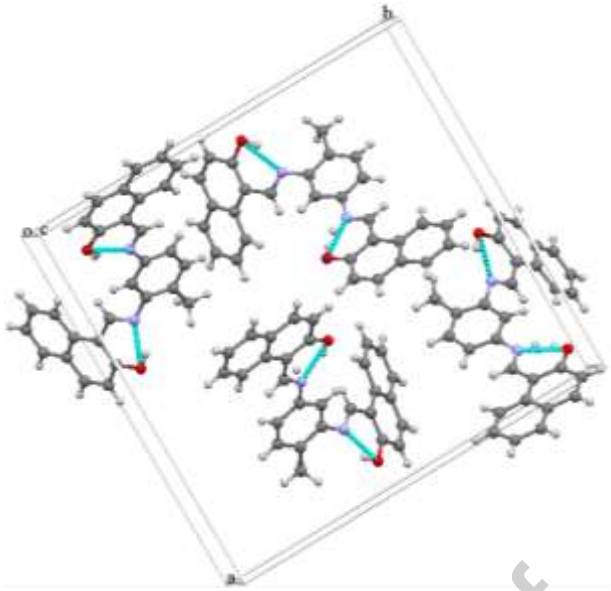

Figure 2. Unit cell of ligand L, provided by intramolecular hydrogen bonds.

Supramolecular 3D-network

The supramolecular 3D-network of the ligand L is enriched by short contacts maintaining the structural cohesion and the stability of the crystal. The supramolecular 3D-network can be seen as the intersection of two sub-networks, the first one is formed by a chains superposition of the molecules in parallel manner with a separation distance of 5.608 Å (Figure 3 a), this parallel molecules are maintained by the short contacts of the types C···C, C···H/H···C, and the second one is formed by helical chiral chains (Figure 3 b) inclined with respect to the first chains by an angle of 28.79 ° (Figure 3 c), the molecules of the helical chiral chains are maintained by the short contacts of the types O···H/H···O and C···H/H···C.

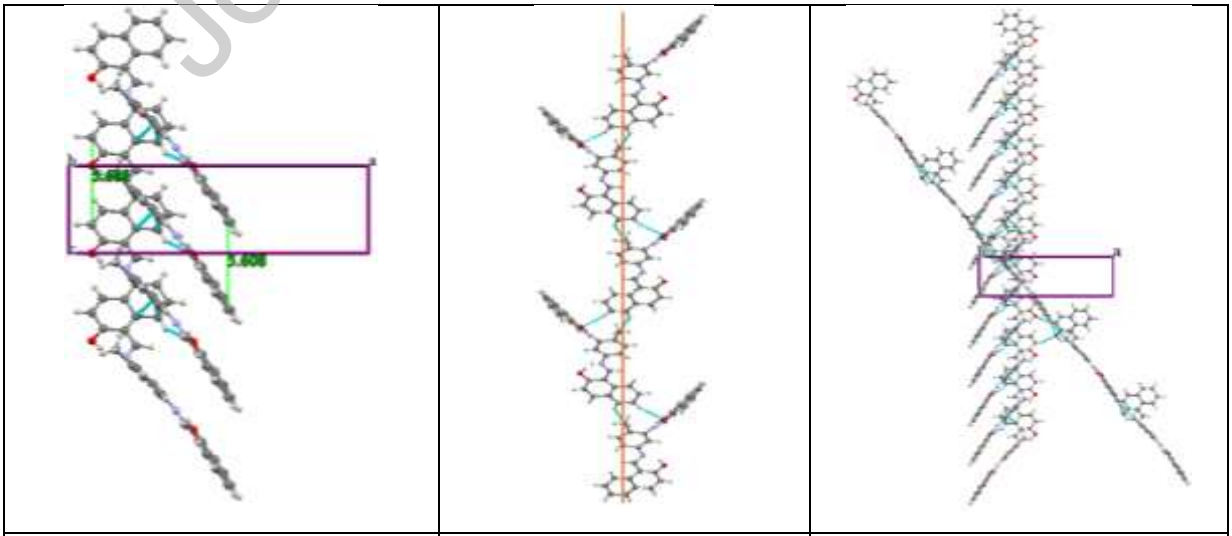

(a) (b) (c)

Figure 3. Supramolecular 3D-network, (a) superposition of the molecules (b) chiral helical chains (c) intersection of the two types of the chains.

3.2. Spectroscopic results

The ligand L was synthesized following standard procedure as shown in the scheme 1 and was characterized by ^{1}H and ^{13}C NMR, IR, UV-Visible and melting point measurements.

3.2.1. ^{1}H-NMR and ^{13}C-NMR analysis

The chemical shifts seen on the peaks of the ^{1}H-NMR spectrum of the ligand L in $DMSO_{-d6}$ is due to the aromatic, the hydroxyl, the imine and the CH_3 group protons (Figure 4). The imine protons of HC=N group appeared as two singlet peaks at 9.74 and 9.79 ppm. The phenolic OH groups showed peak at 15.80 and 16 ppm. Furthermore, the aromatic protons appeared as multiplets and were observed between 7.02-8.58 ppm [10, 30].

The ^{13}C-NMR spectrum, of the ligand L is carried out in the domain 17-175 ppm (Figure 4). The peaks at 171.24 and 172.30 ppm are ascribed to imine carbon atoms C=N functional group [31]. In addition, the peaks due to the phenyl group carbons (C-OH) were observed at 155.73 and 156 ppm and the peak observed at 17.92 ppm can be attributed to the CH_3 attached to the aromatic ring.

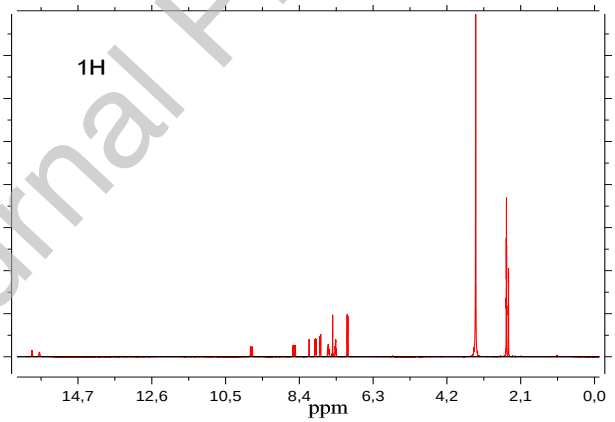

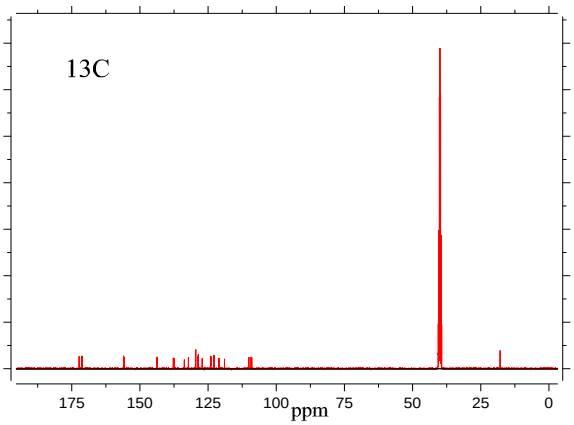

Figure 4. ^{1}H-NMR and ^{13}C-NMR spectra of the ligand L.

3.2.2. FT-IR analysis

Infrared spectrum of the ligand L was recorded in the range of 400-4500 cm^{-1} (Figure 5). A broad band due to hydroxyl group ν(-OH) is observed at 3456 and the band at 1205 cm^{-1} can attributed to the deformation of the phenolic group δ(O-H) [32], while the peaks appearing at 1007, 831, 749 cm^{-1} are referred to aromatic δ(C=C and -CH). Moreover, the formation of the imine bond was confirmed from carbon nitrogen vibration observed for the frequency of 1623 cm^{-1} [3, 33, 34], indicating that the condensation between aldehyde and amine took place. The appearance of band centered at 1247 cm^{-1} is mainly due to the C-O vibration. Finally, the three weak bands observed at 3053, 2921 and 2847 cm^{-1}, are related to the aromatic CH vibration modes [34].

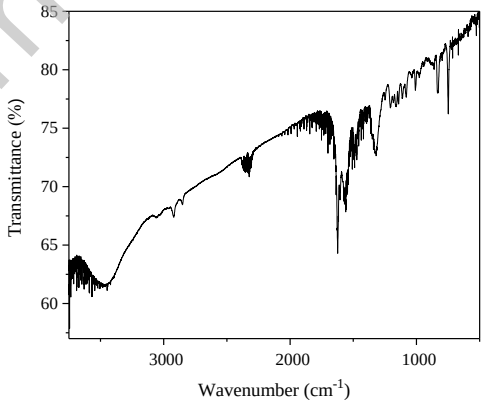

Figure 5. FT-IR spectrum of ligand L.

3.2.3. UV-vis. analysis

The electronic spectrum of the synthesized ligand L was carried out in DMF at room temperature in the range of 200-800 nm (Figure 6). The ligand L exhibits mainly five bands,

which two bands can be observed at 263.17 and 319 nm. The first one located at 263.17 nm can be assigned to the $\pi \rightarrow \pi*$ transitions within the aromatic rings; while the second one located at 319 nm can be attributed to the $n \rightarrow \pi*$ transitions within the azomethine group [33, 35, 36]. Moreover, the bands in the low energy visible region at 393.12, 443.90 and 466.96 nm were assigned to the Ligand Charge Transfer (LCT), these bands could be responsible for the color of L and the extra conjugation between the amine and aldehyde ring [33, 35].

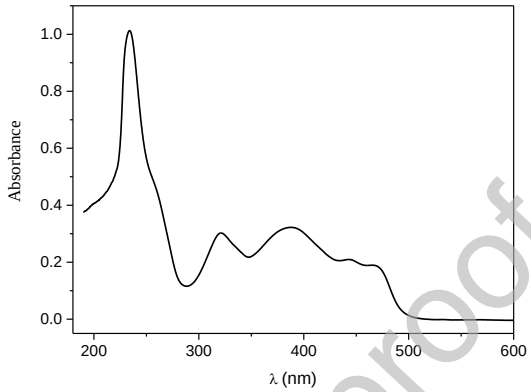

Figure 6. UV-Vis spectrum of the ligand L.

The results of ^{1}H-NMR and ^{13}C-NMR, FT-IR and DRX analysis confirm the structure of the expected product.

3.3. Gravimetric measurement

The gravimetric is a preliminary approach to study the corrosion inhibition. The influence of inhibitor concentration on the inhibition efficiency and corrosion rate for the carbon steel in 1 M HCl solution at room temperature after 24 h of immersion is given in the Table 4.

The corrosion rate (w) and the inhibition efficiency η_w (%) of the studied ligand are determined using the following formulas (9) and (10) [21]:

$$w = \frac{\Delta m}{s.t} \qquad (9)$$

$$\eta_W(\%) = \frac{W0 - Wi}{W0} \times 100 \qquad (10)$$

Where: $\Delta m = m_1 - m_2$

Δm: Masse loss in mg, m_1: initial mass before immersion in mg, m_2: final mass after a time t of the sample immersion in the solution in mg, s exposed surface in cm^2 and t: exposition time in the solution in hour.

w_0 and w_i represent respectively, the corrosion rate values in absence and presence of inhibitor.

Table4
Weight loss results of carbon steel corrosion in 1M HCl at different concentrations of the inhibitor L at 25 °C.

Ligand	Concentration (M)	W_{corr} (mg cm^{-2} h^{-2})	η_w (%)
	Blanc	0,3784	
	5 x 10^{-5}	0,3207	15,24
L	10^{-4}	0,0993	73,75
	5 x 10^{-4}	0,0254	93,27
	10^{-3}	0,0186	95,08

As shown in the Table 4, the inhibition efficiency η (%) increases with the increasing of inhibitor concentration. These behaviors may be ascribed to the enhancive surface coverage of metals, meaning that the active sites of samples are isolated from the aggressive media and further demonstrate that L can act as an effective inhibitor [35].

It is clear that the corrosion rate is decreased obviously compared with that of blank. The maximum efficiency η_w of L is up to 95.08 %. This behavior is the result of increased adsorption of the inhibitor on the metal/surface. In general, L can consider as an effective organic inhibitor, since the tests Gravimetric carried out have shown its ability to inhibit the corrosion of X48 carbon steel.

The plots of the evolution of the corrosion rate and the inhibitory efficiency as a function of the concentration (Figure 7) show that the inhibitory efficiency increases with the increase in the concentration of compound L, on the other hand the corrosion rate decreases.

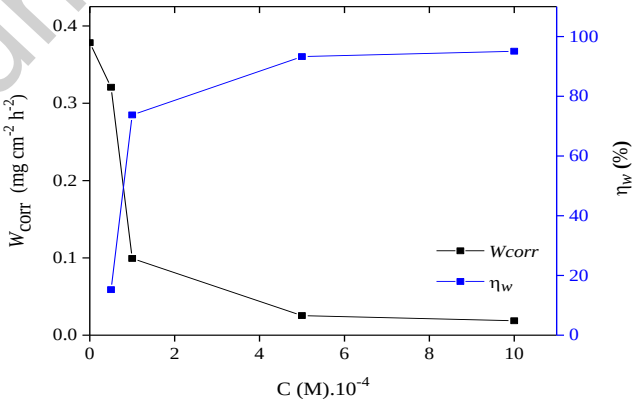

Figure 7. Plots of variation of inhibitory efficiency and corrosion rate with concentration of inhibitor L in 1 M HCl at 25 °C.

3.3.1. Characterization by UV-Vis spectroscopy

UV-Vis spectroscopy is used in several important areas of study, it can provides information on the interactions between inhibitor molecules and carbon steel (X48) [35]. The absorption spectra obtained from a 1 M HCl solution containing 10^{-4} M inhibitor L before and after 24 h immersion of the carbon steel are shown in the Figure 8.

The absorption spectrum of 10^{-4} M of the ligand L (Figure 8) before immersion of the carbon steel show two absorption bands at 357.57 and 321.01 nm. However, after 24 hours of immersion of the carbon steel in the solution, two new absorption bands appear at 290.25 and 276.29 nm less intense than the firsts and we observe the decrease in the intensity of the absorption band at 357.57 nm. This experimental result provide good proof for interaction formed between Fe^{2+} and inhibitor L in 1 M HCl solution [37, 38].

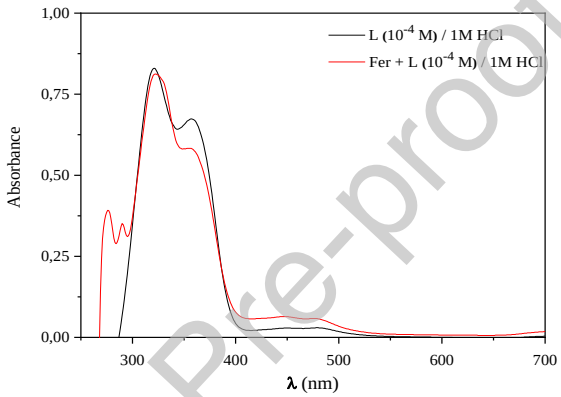

Figure 8. UV-Vis spectra of inhibitor L and the resulting solutions after 24 h of carbon steel immersion.

3.4. Electrochemical Impedance Spectroscopy (EIS)

The Electrochemical Impedance Spectroscopy (EIS) is an efficient method for studying corrosion phenomena at metal/solution interface. The electrochemical impedance diagrams of carbon steel in 1 M HCl in the absence and presence of different concentrations of ligand L is represented in the Figure 9.

Comparable results have been described in literature for the corrosion in acid media of iron and steel in the presence and absence of inhibitor molecule [39].

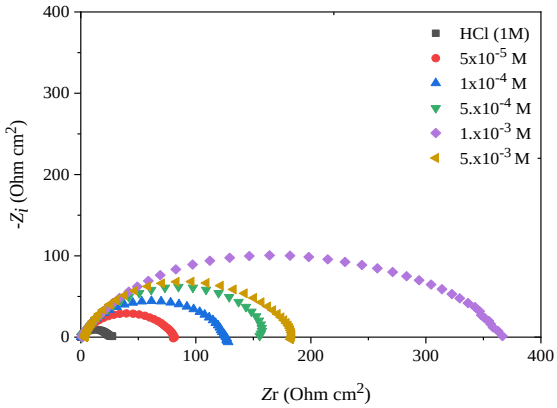

Figure 9. Nyquist plots for different concentrations of inhibitor L in 1 M HCl solution at 25°C.

These curves show that all the Nyquist plots obtained are almost semi-circular and their diameter increases with increasing inhibitor concentration. This indicates that the impedance of an inhibited substrate increases with the increasing of concentration. This result confirms that carbon steel X48 corrosion in HCl medium with and without inhibitor is mainly controlled by charge transfer process [5]. This fact is due to the improved surface coverage of inhibitory molecules on the electrode area.

The capacitive loops are not perfect semicircles; this can be attributed to the frequency dispersion of interfacial impedance arising from the surface roughness, impurities, dislocations, grain boundaries, adsorption of inhibitors, and the formation of porous layers in the electrode surface [40].

The traced Bode diagrams (Figure 10) clearly show that there is single constant phase element at the metal/solution interface. The increase of the absolute impedance in the low frequencies region on the Bode diagrams confirms the inhibitory action of L at high concentrations. This phenomenon indicates that the L inhibitor is adsorbed on the metal surface and form barrier layers and retard corrosion [41, 42].

To establish a model for the carbon steel/solution interface in the presence and absence of the synthesized ligand, the obtained EIS data were fitted by Randles electrical equivalent circuit (Figure 11). Which is a parallel combination of the charge-transfer resistance (R_{ct}) and the constant phase element (CPE), both in series with the solution resistance (R_s).

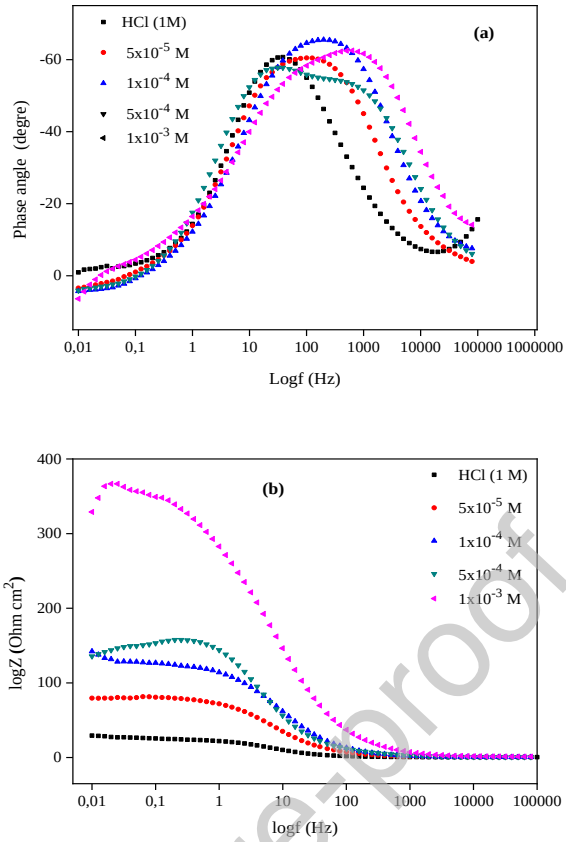

Figure 10. Phase angle (a) and Bode (b) plots for carbon steel in 1M HCl in the presence and absence of different concentrations of inhibitor L at 25 °C.

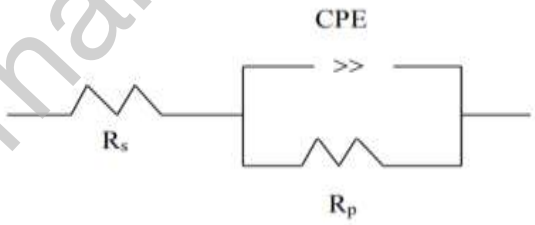

Figure 11. Electrochemical equivalent circuit used for simulation of the impedance spectra.

Double layer capacitance values were obtained at maximum frequency ($f$max), at which the imaginary component of the Nyquist plot is maximum and calculated using the following formula.

$$Cdl = \frac{1}{2\pi\, f\max} \times \frac{1}{Rct} \qquad (11)$$

Where, Rct is inversely proportional to the corrosion current densities.

The inhibition efficiency (η_z %) was calculated from the values the charge transfer resistance (Rct) using the following formula:

$$\eta_z\% = \frac{Rcti - Rct0}{Rcti} \times 100 \qquad (12)$$

R_{ct0} and R_{cti} are respectively the charge transfer resistance values of carbon steel after immersion in absence and in presence of inhibitors.

The impedance parameters: solution resistance, charge transfer resistance R_{ct} and double-layer capacitance C_{dl} values for various concentrations of L in 1 M HCl medium are listed in the Table 5.

Table 5
Impedance parameters and inhibition efficiency values for carbon steel X48 after 30 min immersion period in 1 M HCl solution with and without addition of various concentrations of inhibitor L at 25 °C.

Compound	Concentration (M)	R_s (Ω cm^2)	R_{ct} (Ω cm^2)	C_{dl} (μF cm^{-2})	η_z (%)
HCl	1	0,49	25,79	1232,74	-
1M HCl+ L	5×10^{-5}	0,71	80,51	394,73	67,96
	10^{-4}	0,67	126,3	199,48	79,58
	5×10^{-4}	0,73	158,5	117,86	83,72
	10^{-3}	1,03	342,2	92,87	92,46
	5×10^{-3}	3,41	178,8	112,03	85,57

The Data in the Table 5 show that the effectiveness of the inhibition was increased by increasing the concentration of the inhibitor L up to 10^{-3} M in a 1 M HCl solution and that the Rs values are very small in comparison with the R_{ct} values.

It is observed that the values of charge transfer resistance R_{ct} were increased and the capacitance values C_{dl} decreased with increasing inhibitor concentration. The decrease in the capacitance can result from the decrease of the local dielectric constant and/or the increase in the thickness of the electrical double layer, suggests that the inhibitor molecules act by adsorption process at the metal/solution interface [43].

The inhibitor molecules also reduce the capacitance through the increase in the double layer thickness. The thickness of this protective layer increases with the increase of the inhibitor concentration, resulting a decrease in C_{dl}. This result is in good agreement with the expression of the capacity of the double layer presented in the Helmotz model: $C_{dI} = \frac{\varepsilon_\circ \varepsilon}{d} A$

Where, d is the thickness of the protective layer, ε is the dielectric constant of the medium, ε_0 is the vacuum permittivity and A is the effective surface area of the electrode.

The adsorption of inhibitors on the surface of carbon steel can occur directly based on a donor-acceptor interaction between the double bonds, the phenyl rings and/or the vacant d-orbitals of the surface atoms of the steel. Adsorption can also occur in the cationic form with a positively charged part of the molecule oriented towards the negatively charged metal surface. This confirms the observed decrease in C_{dl} values in the EIS measurement at the corrosion potential [43].

These results confirm also that the corrosion of carbon steel in 1M HCl solution is controlled by a charge transfer Process.

3.5. Polarization measurements

The Figure 12 shows the anodic and cathodic polarization curves recorded on carbon steel electrode in 1 M HCl, in absence and presence of different concentrations of L inhibitor after 30 min of immersion and at room temperature (25 °C). The anodic and cathodic branches of the polarization curves shifted towards lower current density for all investigated concentrations. This indicates that the both of the anodic and cathodic reactions (metal dissolving and hydrogen evolution) were inhibited by Schiff base L in 1 M HCl solution.

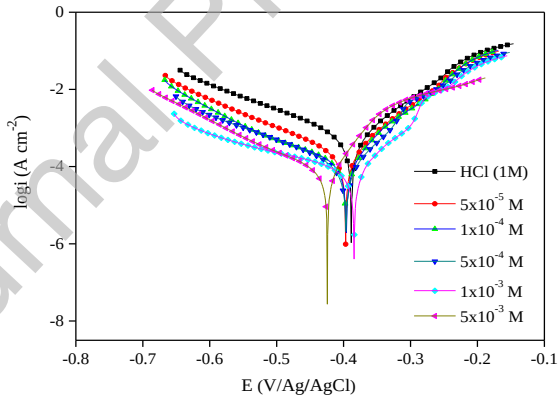

Figure 12. Tafel plots for different concentrations of inhibitor L in 1 M HCl solution.

The electrochemical parameters: corrosion potential (E_{corr}), corrosion current density (i_{corr}) and cathodic and anodic Tafel slopes (b_c and b_a) obtained from polarization curves, and also the corresponding inhibition efficiency (η_p(%)) values for different inhibitor concentrations are given in the Table 6.

The inhibition efficiency, η_p (%), was calculated from the following formula:

$$\eta p\ (\%) = \frac{i^o_{corr} - i_{corr}}{i^o_{corr}} \times 100 \qquad (13)$$

Where, i_{corr}^{o} and i_{corr} are the corrosion current densities without and with the inhibitor, respectively [17].

Table 6.

Polarization parameters and inhibition efficiency values after 30 minutes immersion period in 1 M HCl in absence and presence of different concentrations of inhibitor L at 25 °C.

compound	Concentration (M)	$-E_{corr}$ (mV/Ag/AgCl)	i_{corr} (mA cm^{-2})	b_a (mV/dec)	$-b_c$ (mV/dec)	η_p (%)
HCl	1	389	0,516	83,8	128,6	-
HCl+L	5 x 10^{-5}	397,0	0,210	76,8	143,3	59,30
	10^{-4}	396,1	0,136	71,1	164,5	73,64
	5 x 10^{-4}	396,4	0,115	70.2	158.7	77,71
	10^{-3}	384,4	0,073	63,5	219,9	85,85
	5 x 10^{-3}	424,0	0,081	52,1	152,0	84,30

The addition of the inhibitor is translated by a decrease of the current densities. This shows that the inhibitor is adsorbed on the metal surface. The higher concentration of the inhibitor leads to an elevated inhibition efficiency caused by a higher coverage of inhibitor on the surface. This result suggests that the addition of the synthesized inhibitor reduces anodic dissolution of iron ($Fe \rightarrow Fe^{2+} + 2e^-$) and also retards the hydrogen evolution reaction ($2H^+ + 2e^- \rightarrow H_2$).

The inhibitor causes change in the anodic and cathodic Tafel slopes and no definite trend was observed in the shift of E_{corr} values in the presence of different concentrations of the synthesized inhibitors. According to the literature, if the shift of E_{corr} compared with the blank is lower than 85 mV/SCE, the inhibitor can working as a mixed type [44]. Suggesting that this ligand L behave as mixed type inhibitor.

The best inhibition efficiency was about 85.85 % in 1 M HCl at concentration 10^{-3} M. It can be noted that the inhibitor provides a better inhibitive efficiency.

3.6. Adsorption isotherm

The adsorption isotherm was used to have more insights into the mechanism of corrosion inhibition, since it describes the molecular interaction between the inhibitor molecule and the active sites on the carbon steel surface [17, 45].

It is essential to know the mode of adsorption which the fit of adsorption isotherm can provide an idea. Several types of adsorption isotherm (Frumkin, Temkin and Langmuir isotherm) were tested, the most suitable isotherm corresponds to the maximum correlation coefficient (R^2), which was Langmuir model, the Figure 13 shows the fit with this last model.

The adsorption equilibrium constant (K_{ads}) and free energy of adsorption ($\Delta G°_{ads}$) were calculated using the relations:

$$K_{ads} = \frac{1}{C_{inh}} \times \frac{\Theta}{1-\Theta} \quad (14)$$

$$\frac{C_{inh}}{\theta} = \frac{1}{K_{ads}} + C_{inh} \quad (15)$$

$$K_{ads} = \frac{1}{55.5} Exp\left(\frac{-\Delta G^{o}_{ads}}{RT}\right) \quad (16)$$

$$\Delta G^{o}_{ads} = -2.303RTlog(55.5K_{ads}) \quad (17)$$

Where, θ is the fractional surface coverage, C_{inh} is the inhibitor concentration, K_{ads} is the equilibrium constant, R is the universal gas constant, T is the temperature, and the numerical value 55.5 represents the molar concentration of water in the acid solution.

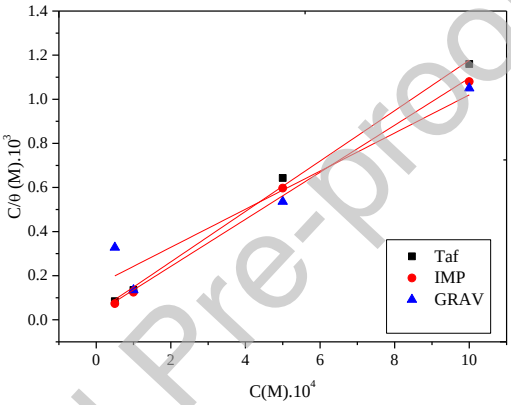

Figure 13. Langmuir's isotherm for the adsorption of inhibitor L on the surface of carbon steel in 1M HCl solution using different methods.

The values of adsorption constant, slope, and correlation coefficient (R^2) can be obtained from the regressions between C_{inh}/θ and C_{inh}, and the results are listed in the Table 7.

Table 7
Thermodynamic parameters for the adsorption of ligand L in 1 M HCl on the Carbon steel at 25 °C.

Methods	R^2	$K_{ad}.10^{-3}$ (M^{-1})	ΔG_{ads} ($kJ.mol^{-1}$)
Gravimetric	0.8978	6.415	-31.69
Tafel	0.9962	29.29	-35.46
Impedance	0.9963	34.94	-35.89

The result shows that all the linear correlation coefficients and all the slopes are close to one, this confirm that the adsorption of the Schiff base L follows the Langmuir adsorption isotherm model.

The thermodynamic parameters for the adsorption process obtained from Langmuir fit show that the negative values of $\Delta G°_{ads}$ and the higher values of K_{ads} reveal the spontaneity of adsorption process and they are characteristic of strong interaction and stability of the adsorbed layer on the steel surface.

Generally, if the values of $\Delta G°_{ads}$ are -20 kJ mol^{-1} or less negative, indicates that the interaction of charged molecule and charged metal surface is electrostatic in nature (physisorption), for values of $\Delta G°_{ads}$ between -20 kJ mol^{-1} and -40 kJ mol^{-1}, so both physical and chemical adsorptions are involved in the inhibitor adsorption process on the metal substrate. If its value is more negative than -40 kJ mol^{-1}, it indicates the presence of coordinate type bond between inhibitor molecules and metal surface (chemisorption) [37, 46]. The calculated $\Delta G°_{ads}$ value varies between -31.69 and -35.89 kJ mol^{-1} implying that the adsorption behavior of the inhibitor L involves both physical and chemical interactions [47, 48]. $\Delta G°_{ads}$ value being closer to -40 kJ mol^{-1}, therefore chemical adsorption is more important than physical adsorption.

It may be assumed that L interacts on the metal mainly through aromatic rings, OH phenol and azomethine.

3.7. Temperature effect

The effect of the temperature on the corrosion of carbon steel against solutions of HCl in the absence and presence of inhibitor L gives insight knowledge on the possible mechanism of inhibitor adsorption. In this way, the polarization experiments were undertaken at 10 °C intervals in the temperature range 25-55 °C considering the absence and presence of inhibitor at 10^{-3} M (Figure 14). This study determines the activation energies, enthalpies and entropies of activation of the corrosion process, and this provides information on the mechanism of inhibition.

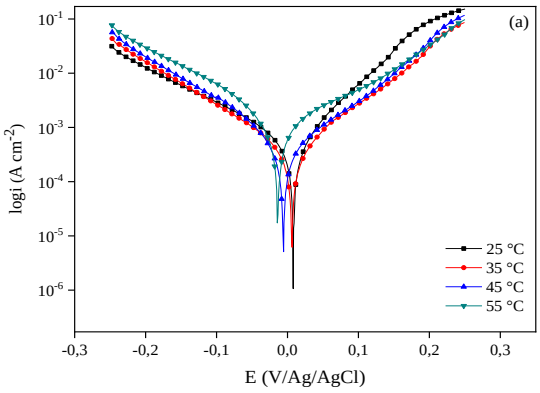

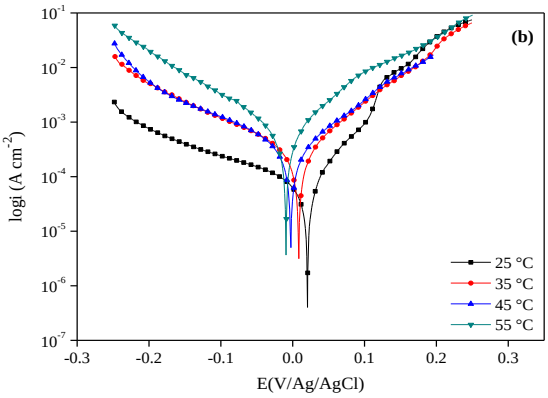

Figure 14. Tafel curves for the corrosion of carbon steel in 1M HCl (a) in the absence and (b) presence of 10^{-3}M of L at different temperatures.

The values of the electrochemical parameters and of the inhibitory efficiencies associated with the corrosion of carbon steel in 1 M HCl in the absence and the presence of 10^{-3} M of ligand L at various temperatures are given in the Table 8.

Table 8
Electrochemical characteristics of corrosion of carbon steel in 1M HCl at different temperatures.

concentration (M)	T (°C)	$-E_{corr}$ (mV/Ag/AgCl)	i^0_{corr} (mA cm^{-2})	$-E_{corr}$ (mV/(Ag/AgCl))	i_{corr} (mA cm^{-2})	η_p (%)
10^{-3}	25	389,0	0,516	384,4	0,073	85,85
	35	446,1	0,528	441,0	0,084	84,09
	45	463,2	0,566	467,0	0,102	81,97
	55	481,0	0,661	472,0	0,146	77,91

The results indicate that the current densities of carbon steel in uninhibited and inhibited acid increased as the temperature increased. However, the extent of the current density in the inhibitor-free acid was higher than the one in the presence of inhibitor L.

It is noted that the inhibition efficiency did not decrease very much with the temperature enhancement, suggesting that the adsorption-desorption equilibrium was not completely shifted towards desorption, and that a protective layer of the inhibitors remained on the surface [5].

The molecules over the metal surface are becoming shorter with the increase of the temperature. Hence, the metal surface remains exposed to the acid environment for longer period, therefore the inhibition efficiency falls at elevated temperature [49].

3.7.1. Determination of activation parameters

The kinetic parameters of the activation for the corrosion of carbon steel in acid with and without the inhibitor L, such as energy (Ea) and pre-exponential factor (A) can be evaluated from the effect of temperature using an Arrhenius-type equation.

$$i_{corr} = \mathrm{Aexp}(\frac{-\mathrm{E_a}}{\mathrm{RT}}) \qquad (18)$$

Thermodynamic characteristics of the corrosion reaction such as: the enthalpy (ΔH°a) and entropy (ΔS°a) were calculated by the transition state equation given below:

$$i_{corr} = \frac{RT}{Nh} \exp\left(\frac{\Delta S_a^\circ}{R}\right) \exp\left(-\frac{\Delta H_a^\circ}{RT}\right) \qquad (19)$$

Where: *h* is the Planck's constant, *N* is the Avogadro number, *R* is the universal gas constant, *T* is the temperature, $\Delta H°_a$ is the enthalpy of activation and $\Delta S°_a$ is the entropy of activation.

The Figure 15 shows the plots of $\log i_{corr}$ as a function 1/T. Straight lines are obtained, having the slopes (Ea/R) and the intercepts logA.

The Figure 16 shows the plots of log (i_{corr}/T) as a function 1/T in the absence and presence of L for a temperature range of (298 - 328K).

ΔH° and ΔS° were computed from straight lines, which has a slope equal to -ΔH°/2.303R and an intercept ((log R/Nh) + ΔS°/2.303R), and the results are listed in the Table 9.

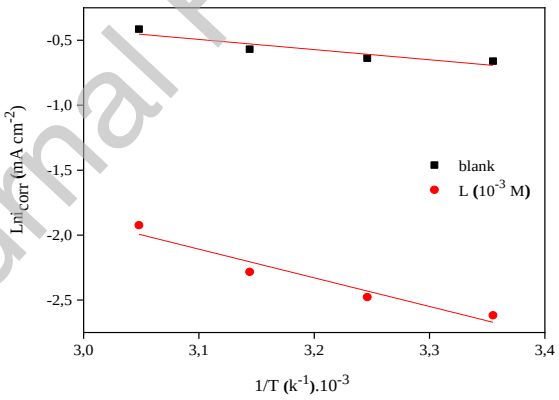

Figure 15. Arrhenius plots for the corrosion of XC48 steel in 1M HCl in absence and presence of 10^{-3} M of L at different temperatures.

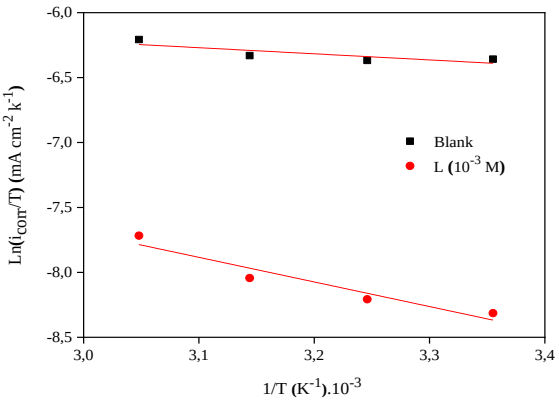

Figure 16. Transition state curves for the corrosion of XC48 steel in 1M HCl in the presence and absence of 10^{-3} M of L at different temperatures.

Table 9
Activation parameters of the dissolution of carbon steel in 1 M HCl in the absence and presence of 10^{-3} M of L.

Concentration	E_a ($kJ.mol^{-1}$)	ΔH^0_a ($kJ.mol^{-1}$)	$\Delta S°_a$ ($J.mol^{-1}$)
1 M HCl	6.50	3.90	-237.40
HCl + L 10^{-3} M	18.33	15.73	-214.12

In the literature the inhibitors for which the activation energy of the inhibited solution is greater than that of the blank solution are adsorbed on the substrate by electrostatic bonds (physisorption) and the inhibitors which have the activation energy (E_{inh}) lower than that of the blank solution are adsorbed on the metal surface by strong bonds (chemisorption) [50, 51]. The increase in the value of the activation energy in the presence of the ligand implies that the adsorption of this inhibitor on the surface of the steel is due to bonds of an electro-static nature (physisorbed on the surface of the electrode) and that the dissolution of carbon steel was decreased due to the formation of a barrier by the adsorption of the inhibitor on the metal surface [12] suggesting the formation of a multilayer film.

- The positive signs of the enthalpies ΔH^0_a reflect the endothermic nature of the steel dissolution process [52].

- The high and negative values of the entropy $\Delta S°_a$ mean that the disorder is reduced when the reagents are converted into activated iron-molecule complex in solution [53, 54].

3.7.2. Determination of thermodynamic adsorption parameters

The thermodynamic adsorption parameters (K_{ads}, $\Delta G°_{ads}$, $\Delta H°_{ads}$ and $\Delta S°_{ads}$) at the optimum concentration 10^{-3} M in 1 M HCl at the temperature range from 25-55 °C are calculated according to relations (14) and (17) and the plot of the variation of $\Delta G°_{ads}$ as a function of the

temperature (T) (Figure 17) to calculate the standard adsorption enthalpy ($\Delta H°_{ads}$) and entropy ($\Delta S°_{ads}$) the Gibbs-Helmholtz's equation was used (20):

$$\Delta G^{\circ}_{ads} = \Delta H^{\circ}_{ads} - T\Delta S^{\circ}_{ads} \quad (20)$$

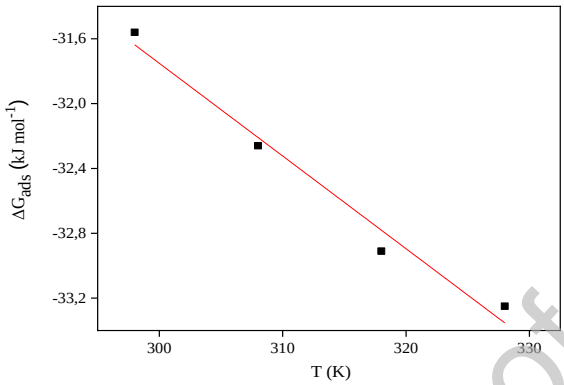

Figure 17. Variation of the standard adsorption free energy (ΔG°ads) as a function of the temperature.

The values of the thermodynamic adsorption parameters Kads, ΔG°ads, ΔH°ads and ΔS°ads are grouped in the Table 10.

Table 10
Thermodynamic parameters for the adsorption of inhibitor L in 1 M HCl on the Carbon steel at 25–55 °C.

Ligand	T (°C)	$K_{ads} . 10^{-3}$ (M^{-1})	$-\Delta G°_{ads}$ (kJ/mol)	$\Delta H°_{ads}$ (kJ/mol)	$\Delta S°_{ads}$ (J/mol.K)
L	25	6.067	31.56	-14.59	-57.2
	35	5.285	32.26		
	45	4.546	32.91		
	55	3.526	33.52		

It is evident seen from the table 10 that the high K_{ads} and $\Delta G°_{ads}$ values for the compound L indicate a strong adsorption of the inhibitor molecules on the metal surface. In the literature the $\Delta G°_{ads}$ value between -20 $kJ.mol^{-1}$ and -40 $kJ.mol^{-1}$ reflects a mixed adsorption combining physisorption and chemisorption [55, 56].

The adsorption for inhibitor is governed by the combination of the both chemisorption and physisorption [52].

The negative sign of $\Delta H°_{ads}$ value confirm that the adsorption of inhibitor L is an exothermic process.

The negative value of the entropy ($\Delta S°_{ads}$) shows that the activated complex present an association step rather than a dissociation step, meaning that a decrease in disordering takes place on going from reactants to the activated complex [9, 57, 58].

3.8. Surface studies by Scanning Electron Microscope (SEM)

The surface morphology of the carbon steel was studied by using Scanning Electron Microscopy (SEM). SEM images of polished bare carbon steel surface, carbon steel immersed in 1M HCl solution in absence and presence of inhibitor at the concentration of 10^{-3} M for 24 hours of immersion at 25 °C are shown in the Figure 18. The surface of polished bare carbon steel is very smooth and shows no corrosion (Figure 18 a). In absence of the inhibitor, the figure 18 b1 exhibits grossly eroded surface with an accumulation of corrosion products. This is a result of direct attack on carbon steel surface by aggressive ions from the acid [59].

On the other hand, in the presence of the inhibitor the figure 18 c confirms that damage on the metal surface is apparently reduced and the surface is smoother contains fewer pits. This confirms that the inhibitor (L) protect the steel surface such that the metal is not exposed to direct attack by acidic ions [60].

The SEM figures confirm the protection of carbon steel against 1 M HCl solution by the studied Schiff base. These results agree well with electrochemical studies.

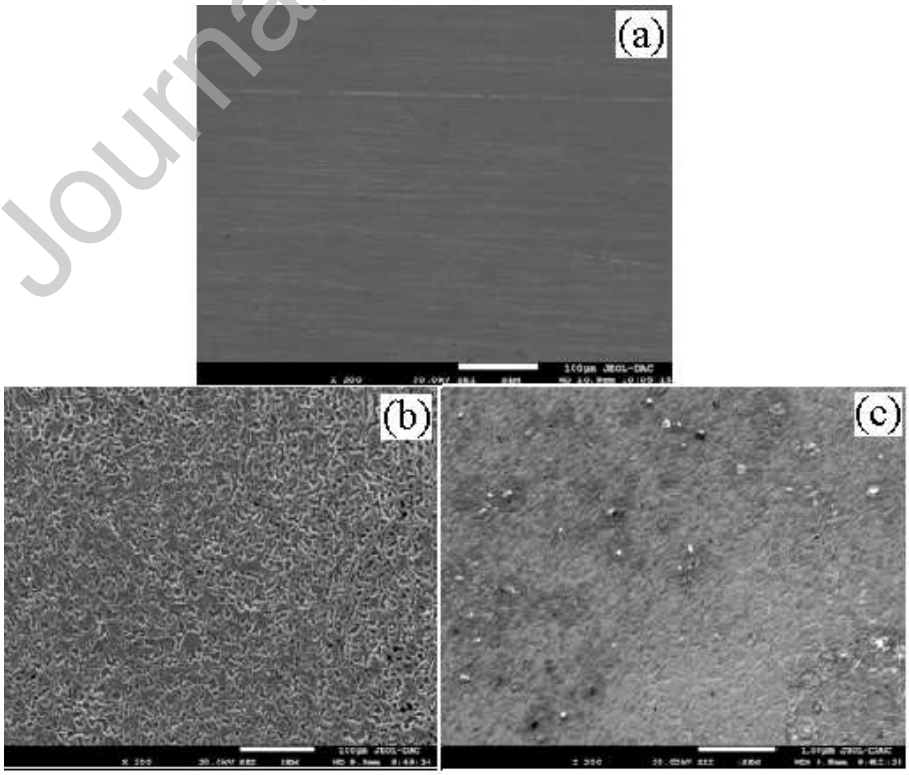

Figure 18. SEM figures of carbon steel samples: (a) polished surface, (b) after 24 hours immersion in 1M HCl, (c) after 24 hours immersion in 1M HCl+10^{-3} M of L.

3.9. Quantum Chemical Studies

To study the effect of the electronic properties and molecular structure towards the inhibition effectiveness of ligand L and to confirm or infirm the experimental data obtained from electrochemical experiments, a quantum chemical calculation has been carried out.

The optimized molecular structure provided by the atomic numbering and the frontier molecular orbital density distributions (HOMO and LUMO) of ligand L given by the B3LYP/6-31G (d,p) method are shown in the Figure19.

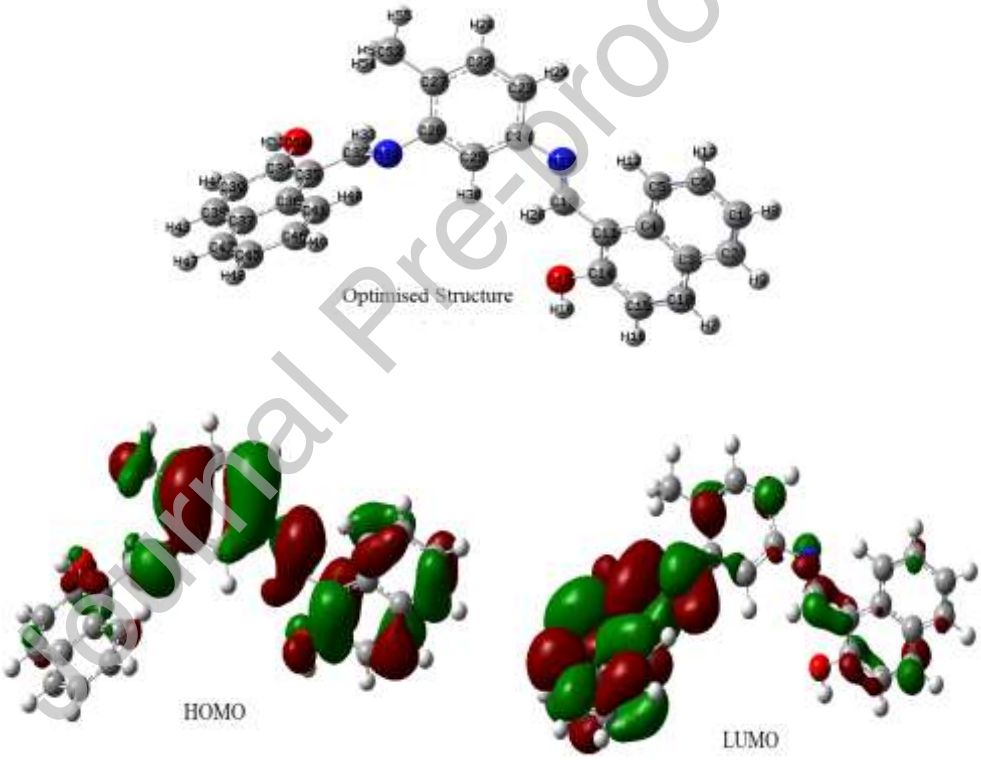

Figure 19. Optimized structure and the frontier molecular orbital density distribution (HOMO and LUMO) of ligand L given by the B3LYP/6-31(d.p.) method.

The figure 19 shows that the electron density of the HOMO is located on almost all of the molecule except a single naphthalene group. Otherwise, the electron density of the LUMO is distributed almost exclusively on the second naphthalene group.

The calculated quantum parameters: the energies of highest occupied molecular orbital (E_{HOMO}) and the lowest unoccupied molecular orbital (E_{LUMO}), the energy variation (ΔE_{gap})

between E_{HOMO} and E_{LUMO}, the absolute electronegativity (χ), dipole moment (μ), global hardness (η), the portion of electrons transported (ΔN), the total energy (E_{Tot}) are presented in the Table 11.

Table 11.
Calculated parameters for the studied L inhibitor in the gas and aqueous phase obtained using the DFT method at the B3LYP/6-31G(d,p) basis set.

Quantum parameters	Gas phase	Aqueous phase
E_{tot} (eV)	-37506.02	-37506.56
E_{HOMO} (eV)	-5.19	-5.46
E_{LUMO} (eV)	-1.65	-1.87
ΔE_{GAP} (eV)	-3.54	-3.59
μ (Debye)	5.25	9.40
η (eV)	1.77	1.80
σ (eV^{-1})	0.565	0.557
χ (eV)	3.42	3.67
ω (eV)	3.30	3.74
ΔN	1.01	0.93

The table 11 reveals that the value of E_{HOMO} of L is high and the value of E_{LUMO} is low, which confirm the inhibition efficiency obtained experimentally [61].

The high value of E_{HOMO} (-5.19 eV) is due to the presence of electron donating of CH_3 and OH groups attached to phenyl ring. Furthermore, the low value of E_{LUMO} (-1.65 eV) suggests that L has a high capacity for accepting electrons [62].

Energy gap (ΔE) is an important parameter that reveals activity of an inhibitor molecule. The low value of ΔE (-3.54 eV) demonstrate higher reactivity and facilitate adsorption of the organic molecule on steel surface, and consequently, higher inhibition performance [63]. The decrease of ΔE and of E_{LUMO} as well as the increase of E_{HOMO} involves the increase of inhibitor efficiency [64]. In addition, the softness is also an important parameter, which can elucidate the adsorption ability of the inhibitor molecules. Higher value of softness and lower value of hardness are associated to the strong interaction with metal and the high inhibition efficiency [65].

The value of the softness is 0.56 and the value of hardness is 1.77, which can predict the good affinity of the adsorption of L, which is in accordance with the experimental results.

Whenever, the value of ΔN is greater than zero and less than 3.6 ($0 < \Delta N < 3.6$) it suggests that the transfer of electrons from an inhibitor to a metal takes place easily [52]. From the table 11, the calculated value of ΔN is 1.01 which clearly shows that the molecules of L have a strong tendency to donate electrons to the vacuum orbital of the metal [66].

Furthermore, the inhibition efficiency increases with the decrease in the value of ω, the ligand L has a low ω value (3.30 eV) which confirms its high inhibitory efficacy. Otherwise, the electronegativity values (χ) are decisive. A lower value of this quantum parameter (χ = 3.42 eV) is favorable for the high inhibition efficiency [67].

The dipole moment (μ) is the parameter most used to describe the polarity of a molecule. It is clearly proved in the literature that molecules with high dipole moments and greater than the dipole moment of H_2O (1.88 Debye), are more reactive [65]. In our study, the high value of the dipole moment of L is 5.25 Debye in the gas phase and 9.40 Debye in the aqueous phase confirm the high reactivity, so the absorption of inhibitory molecules on the metal surface may becomes strong [47].

Molecular Electrostatic Potential (MEP)

Molecular Electrostatic Potential (MEP) being related to electron density, it is a useful descriptor for determining the sites of electrophilic and nucleophilic reactions.

From the Figure 20, the most electrostatic potential, indicated by the yellow color, occupies almost the entire center of the molecule, concentrated around the two C = N bonds suggesting a huge electron deficit and therefore a possible center of active electrophilic regions. This clarifies the fact that ligand L is predominant towards electrophilic attack and therefore has a high capacity of binding to the metal surface. On the other hand, the active nucleophilic sites are located around the oxygen of the hydroxyl group.

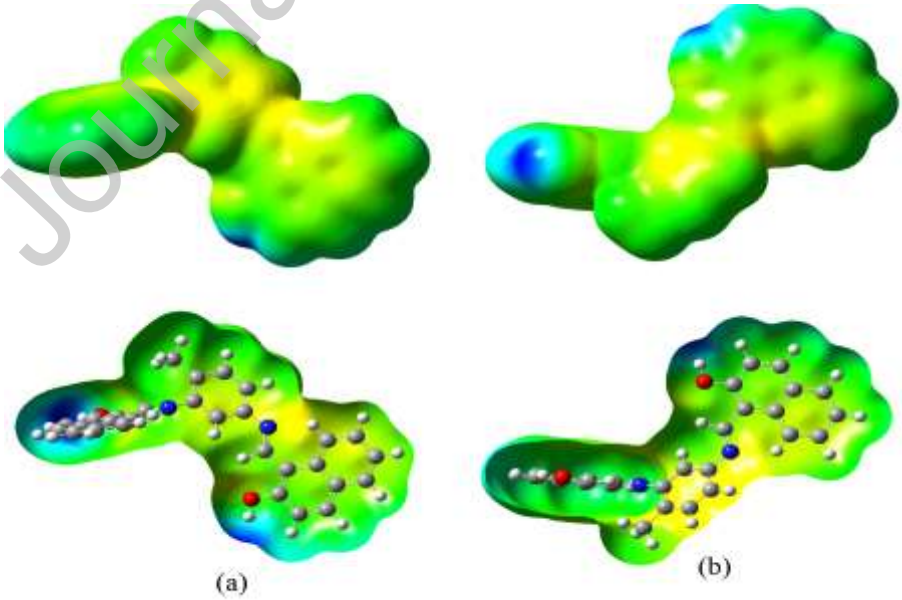

Figure 20. MEP and counter plot of the studied inhibitor L (a) Front view and (b) Rear view.

The Mulliken charge of the molecule evaluates the way how the atomic displacement affects the electronic structure [68].

Mulliken atomics charges distribution of L molecule are given on the Figure 21 the atoms carrying negative charges are the negative charge centers, which can offer electrons to the Fe atoms to form coordinate bond, and the atoms carrying positive charges are the positive charge centers, which can accept electrons from orbital of Fe atoms to form feedback bond.

From the Figure 21, the results reveal that, the most negative charge in the studied compound is resident in the nitrogen and oxygen atoms (O (17) −0.56018; O (50) −0.56096; N (21) −0.51528 and N (31) −0.49437) [69].

So we observe that the oxygen and nitrogen atoms play an important role in the adsorption process of molecule on carbon steel surface through a donor-acceptor type reaction [70].

The Mulliken charges of the atoms indicate that the most negative atoms are active adsorptive centers. This agrees perfectly with the literature results [71].

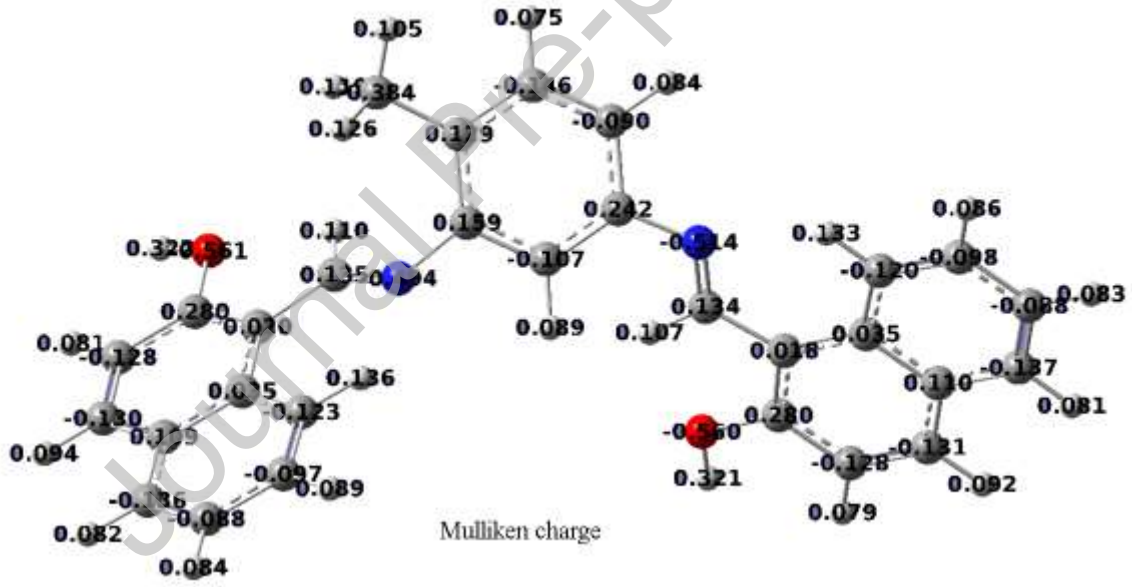

Figure 21. Mulliken charges density and of L given by the B3LYP/6-31(d.p.).

Molecular Dynamic Simulations are a good way to improve knowledge on the study of corrosion inhibition and the molecular interactions between the inhibitor molecules and metal surface.

The equilibrium adsorption configurations obtained from the neutral form of the inhibitor L on the surface of Fe (110) in solution and in the gas phase are shown in the Figure 22. It can

be seen that the inhibitor L is adsorbed on carbon steel surface in a parallel form by increasing the surface coverage [72], but with an orientation of inhibitor molecule directed away from the Fe surface in some part of the structure moiety [64].

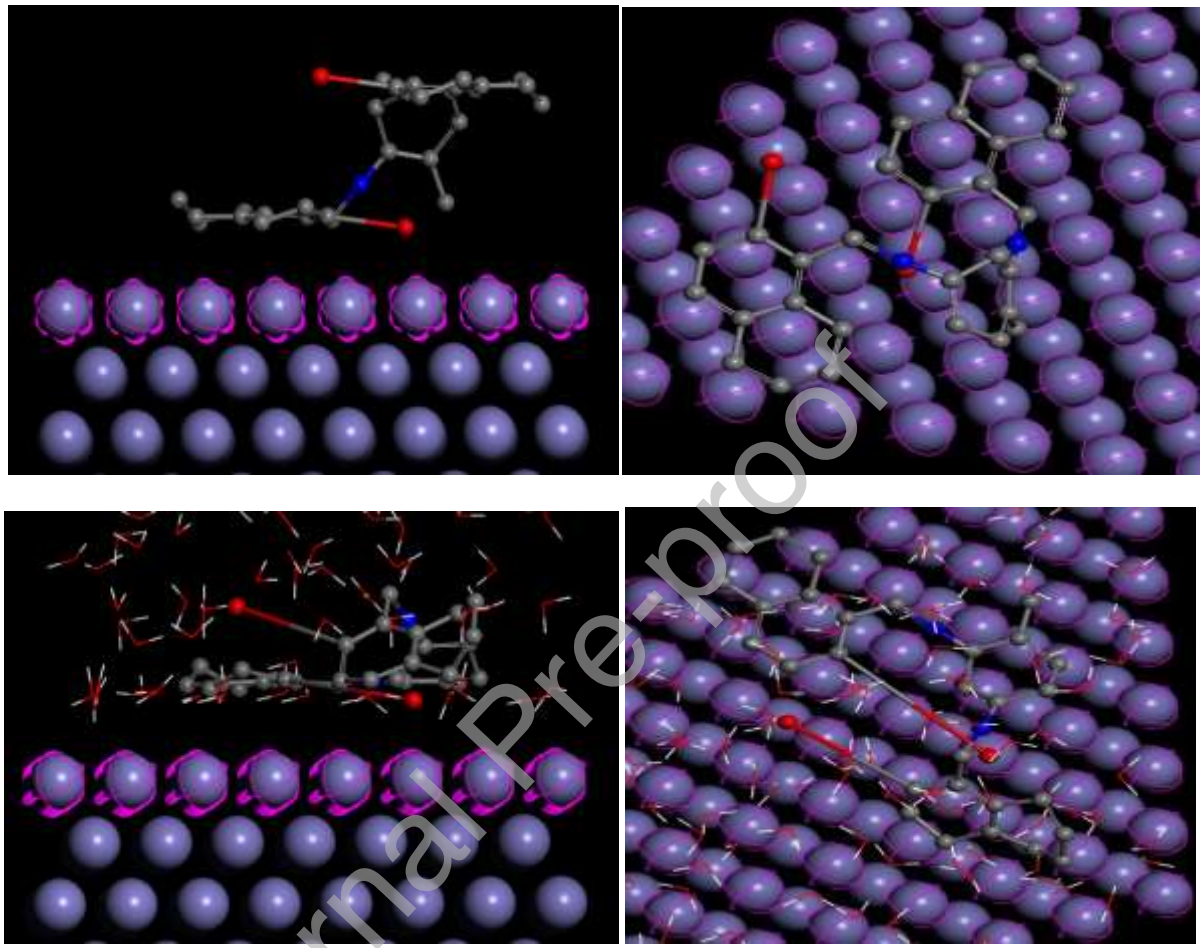

Figure 22. Side views and top views of the most stable configurations for adsorption of L on Fe (110) surface calculated using Monte Carlo simulations in the gas phase and aqueous phase.

The molecular dynamics simulations data proved that inhibitor could adsorb on steel surface through the p-electrons of rings and the free lone-pair electrons in heteroatom's.

The results of the simulation energies namely total energy (E_{tot}), adsorption energy (E_{ads}) and deformation energy (E_{def}) are summarized in the Table 12.

It is important to note that higher negative adsorption energy values indicate a more stabilized interaction between inhibitors and iron surfaces [52].

It is clear that the total energy, the strain energy and the adsorption energy increase when passing from the gaseous state to the liquid state. This confirms that the protonated form of inhibitor would absorb more strongly to the surface of iron than the neutral form.

The computed interaction energy of the adsorption systems showed that the tested inhibitor is greatly adsorbed on the Fe surface in the aqueous solution and the high negative value of interaction energy value is attributed to strong adsorption of the molecules on the Fe surface. Finally, it can be concluded that the theoretical results agree well with the experimental results.

Table 12
Energy values calculated between the inhibitor L and the Fe (110) surface in the absence and presence of water.

System	inh/Fe (110)	inh/Fe (110)/H_2O
Total energy (kcal mol^{-1})	-201	-1171
Adsorption energy (kcal mol^{-1})	-923	-3644
Deformation energy (kcal mol^{-1})	-732	-2660

Generally, when the distances of the bonds between the iron atom and the heteroatom's of the inhibitory molecules are in the interval of 1 Å ~ 3.5 Å, the chemical bonds can be formed, while the physical interactions are associated with the distances longer than 3.5 Å [73].
As shown in the Table 13, the distance between Fe---L (Fe---O17 and Fe---N21) is less than 3.5 Å, indicates the chemisorption in the inhibition process in the aqueous solution, but the distances between Fe---O50 and Fe---N31 are longer than 3.5 Å, suggesting that the physisorption could be involved in the inhibition process. In addition, the found coordination bonds are due to the existence of non-binding electrons located on the nitrogen and oxygen of the hydroxyl group atoms. These results confirm the chemisorption and physisorption of inhibitory molecule.

Table 13
Distance between heteroatoms inhibitory molecules and iron atoms on the plane (1 1 0).

ligand	System	Distance (A˚) inh/Fe	Distance (A˚) inh/Fe/H_2O
L	Fe---O17	2,5	2
	Fe---O50	7,5	5,2
	Fe---N21	4	2,5
	Fe---N31	7	4,7

Finally, the results given by the MDS are in good agreement with the experimental results. Quantum chemical calculations clarified the relation between structural parameters of the studied compound and their inhibition efficiency for the corrosion process.

Conclusion

According to the results obtained in this study, we can get the following conclusions:

- Schiff base, 2,4- Bis (2-hydroxy naphthaldehyde) diiminotholuene (L), was synthesized and their molecular structure was confirmed by X-Ray diffraction on single crystal, ^{13}C-NMR, ^{1}H-NMR, UV-Vis and FT-IR spectroscopies.
- Prepared Schiff base L showed that the inhibition efficiency increases with the increase of inhibitor concentration, and attains a maximum value at 10^{-3} M.
- Electrochemical impedance spectroscopy results showed that double layer capacitances (C_{dl}) decrease with respect to blank solution when Schiff base L added but charge transfer resistances (Rct) increase. This fact may be explained by the adsorption of L molecules on the steel surface.
- Potentiodynamic polarization measurements indicate that the Schiff base L act as mixed type inhibitor controlling both cathodic and anodic reactions.
- Adsorption of this compound on carbon steel surface in 1 M HCl obeyed to Langmuir adsorption isotherm and the values of ΔG^{o}_{ads} revealed that the adsorption mechanism of this inhibitor is mainly dominated by physical and chemical adsorption.
- Study of the temperature effect shows that the inhibition efficiency decreases slightly with the increase of the temperature, which confirms that the adsorption of the inhibitor L on the surface occurs through physisorption and chemisorption.
- UV-Vis spectroscopy provides good proof for interaction formed between Fe^{2+} and Schiff base L inhibitor in 1 M HCl solution, confirming the formation of protective layer of metal-inhibitor on carbon steel surface.
- SEM analysis showed that the presence of the inhibitor in the corrosive solution change the corrosion morphology caused by HCl. The SEM figures proved the formation of the adsorbed inhibitor layer protective against the corrosion.
- DFT calculations, Monte Carlo dynamic simulations are in excellent agreement with the experimental findings.
- Finally, all analysis proves that the studied Schiff base L is a good inhibitor in the aggressive medium against 1M HCl solution.

Acknowledgement

The Authors would like to thank Professor Lahcene OUAHAB for the help to access the crystallography at Institut of Chemical Sciences of the University of Rennes 1 CDiFX France.

Credit Author Statement

Boukazoula soraya: Synthesis, characterization and elaboration, Interpretation, Methodology and Writing. HAFFAR Djahida: Interpretation, Methodology, Writing - review & editing. TOUKAL Linda: Interpretation, Theoretical calculations. DORCET Vincent: Molecular structure. BOURZAMI Riadh: Interpretation, Methodology and Writing.

Declaration of interests

☒ The authors declare that they have no known competing financial interests or personal relationships that could have appeared to influence the work reported in this paper.

☐ The authors declare the following financial interests/personal relationships which may be considered as potential competing interests:

Reference

[1] P.R. Roberge, Handbook of corrosion engineering. McGraw-Hill, New York, (2000) p 839.
[2] N.K. Gupta, C. Verma, M.A. Quraishi, A.K. Mukherjee, Schiff's bases derived from L-lysine and aromatic aldehydes as green corrosion inhibitors for mild steel: Experimental and theoretical studies, J. Mol. Liq. 215 (2016) 47-57 https://doi.org/10.1016/j.molliq.2015.12.027
[3] A. Kheniche, A. Ourari, A. Dakhouche, A. Ghanem, W. Min, K. Meguellati, Electrochemical and theoretical studies influencing the effect of hydroxyl position of tetraphenolic schiff bases towards corrosion inhibition of mild steel in 1M HCl,
J. Fundam. Appl. Sci. 10(3) (2018) 209-238 http://dx.doi.org/10.4314/jfas.v10i3.16.
[4] C.B. Pradeep Kumar, K.N. Mohana, Corrosion inhibition efficiency and adsorption characteristics of some Schiff bases at mild steel/hydrochloric acid interface, J. Taiwan. Inst. Chem. Eng. 45 (2014) 1031-1042 https://doi.org/10.1016/j.jtice.2013.08.017.
[5] S. Mouzali, D. Haffar, L. Bouzidi, Z. Bouanane, Synthesis, Characterization and Inhibition Effect of a New Schiff Base (E)-3-(((2-amino-4-methylphenyl)imino)methyl) naphthalen-2-ol on the Corrosion of Carbon Steel X48 in acidic medium, Int. J. Electrochem. Sci. 12 (2017) 1042-1063 https://doi: 10.20964/2017.11.65.
[6] M.N. El-Haddad, K.M. Elattar, Synthesis, characterization and inhibition effect of new antipyrinyl derivatives on mild steel corrosion in acidic solution, Int. J. Ind. Chem. 6 (2015) 105-117 https://doi 10.1007/s40090-015-0037-9.
[7] P. Singh, M.A. Quraishi, S.L.Gupta, A. Dandia, Investigation of the Corrosion Inhibition effect of 3-methyl-6-oxo-4-(thiophen-2-yl)-4,5,6,7-tetrahydro-2H-pyrazolo[3,4-b]pyridine-5-carbonitrile(TPP) on mild steel in hydrochloric acid, J. Taibah. Univ. Sci. 10 (2016) 139-147 https://doi.org/10.1016/j.jtusci.2015.07.005.
[8] S. Shahabi, P. Norouzi, M.R. Ganjali, Theoretical and Electrochemical Study of Carbon Steel Corrosion Inhibition in the Presence of Two Synthesized Schiff Base Inhibitors:

Application of Fast Fourier Transform Continuous Cyclic Voltammetry to Study the Adsorption Behavior, Int. J. Electrochem. Sci. 10 (3) (2015) 2646-2662.
[9] I. Ahamad, C. Gupta, R. Prasad, M.A. Quraishi, An experimental and theoretical investigation of adsorption characteristics of a Schiff base compound as corrosion inhibitor at mild steel/hydrochloric acid interface, J. Appl. Electrochem. 40 (2010) 2171-2183 https://doi.org/10.1007/s10800-010-0199-2.
[10] Y. Boughoues, M. Benamira, L. Messaadia, N. Ribouh, Adsorption and corrosion inhibition performance of some environmental friendly organic inhibitors for mild steel in HCl solution via experimental and theoretical study, Colloids Surf A. 593 (2020) 124610 https://doi.org/10.1016/j.colsurfa.2020.124610.
[11] G. Gece, The use of quantum chemical methods in corrosion inhibitor studies, Corros. Sci. 50 (2008) 2981-2992 https://doi.org/10.1016/j.corsci.2008.08.043**.**
[12]Y.E. Louadi, F. Abrigach, A. Bouyanzer, R. Touzani, A. El Assyry, A. Zarrouk, B. Hammouti, Theoretical and Experimental Studies on the Corrosion Inhibition Potentials of Two Tetrakis Pyrazole Derivatives for Mild Steel in 1.0 M HCl, Port. Electrochimica. Acta. 35(3) (2017) 159-178.
[13] C. Verma, M.A. Quraishi, A. Singh, 2-Amino-5-nitro-4,6-diarylcyclohex-1-ene-1,3,3-tricarbonitriles as new and effective corrosion inhibitors for mild steel in 1 M HCl: experimental and theoretical studies, J. Mol. Liq. 212 (2015) 804-812 https://doi.org/10.1016/j.molliq.2015.10.026.
[14] S.M. Tawfik, Corrosion inhibition efficiency and adsorption behavior of N,N-dimethyl-4-(((1-methyl-2-phenyl-2,3-dihydro-1H-pyrazol-4-yl)imino)methyl) Nalkylbenzenaminium bromide surfactant at carbon steel/hydrochloric acid interface, J. Mol. Liq. 207 (2015) 185-194 https://doi.org/10.1016/j.molliq.2015.03.036.
[15] A. Abdelmadjid Madi, D. Haffar, F. Benghanem, S. ghedjati, L Toukal, V. Dorcet, R. Bourzami, Synthesis, Crystal structure, Electrochemical, Theoretical Studies and Antioxidant Activities of New Schiff Base, J. Mol. Struct. 1227 (2021) 129368 https://doi.org/10.1016/j.molstruc.2020.129368.
[16] M. Mahjoobizadeh, R. Takjoo, A. Farhadipour, J.T. Mague, Fe(III), Cu(II) and U(VI) binuclear complexes with a new isothiosemicarbazone ligand: Syntheses, characterization, crystal structures, thermal behavior and theoretical investigations, Inorganica. Chim. Acta. 482 (2018) 643-653 https://doi.org/10.1016/j.ica.2018.07.011.
[17] M. Behpour, S.M. Ghoreishi, N. Soltani, M. Salavati-Niasari, M. Hamadanian, A. Gandomi, Electrochemical and theoretical investigation on the corrosion inhibition of mild steel by thiosalicylaldehyde derivatives in hydrochloric acid solution , Corros. Sci. 50 (2008) 2172-2181 https://doi.org/10.1016/j.corsci.2008.06.020.
[18] M. Frisch, G. Trucks, H. Schlegel, G. Scuseria, M. Robb, J. Cheeseman, J. Montgomery Jr, T. Vreven, K. Kudin, Jc Burant, Gaussian 03, revision c. 02, Gaussian, Inc, Wallingford CT, (2004) p 4.
[19] A.D. Becke, Density functional calculations of molecular bond energies, J. Chem. Phys. 84 (1986) 4524-4529 https://doi.org/10.1063/1.450025.
[20] A.D. Becke, Density-functional thermochemistry. III. The role of exact exchange, J. Chem. Phys. 98 (1993) 5648-5652 https://doi.org/10.1063/1.464913.
[21] C. Lee, W. Yang, R.G. Parr, Development of the Colle-Salvetti correlation-energy formula into a functional of the electron density, Phys. Rev. B 37 (1988) 785-789 https://doi.org/10.1103/PhysRevB.37.785.

[22] M.J. Dewar, W. Thiel, Ground states of molecules. 38. The MNDO method. Approximations and parameters, J. Am. Chem. Soc. 99 (1977) 4899-4907 https://doi.org/10.1021/ja00457a004.

[23] A.D. Khalaji, K. Fejfarova, M. Dusek, A.N. Chermahini, Synthesis, Crystal Structure and Conformational Studies of Schiff-Base Compound 2-{[4-(Phenyldiazenyl)Phenyl] Iminomethyl}-5-Bromophenol. J Chem. Crystallogr. 42 (2012) 136-140 https://doi.org/10.1007/s10870-011-0214-4.
[24] H. Gökce, Y.B. Alpaslan, C.T. Zeyrek, E. Ağar, A. Güder, N. Özdemir, G. Alpaslan, Structural, Spectroscopic, Radical Scavenging Activity, Molecular Docking and DFT Studies of a Synthesized Schiff Base Compound, J. Mol. Struct. 1179 (2019) 205-215. https://doi.org/10.1016/j.molstruc.2018.11.005.
[25] L. Checinska, J. Lewkowski, M. Małecka, M. Dziegielewski, Synthesis and Characterization of N,N'-terephthalidenebis(o-aminoaniline): Crystal Structures of Its Two Polymorphic Forms Controlled by Changing the Crystallization Solvent, J. Chem. Crystallogr. 43 (2013) 421-428 https://doi.org/10.1007/s10870-013-0439-5.
[26] M. Sánchez, O. Sánchez, H. Höpfl, M.E. Ochoa, D. Castillo, N. Farfán, S. Rojas-Lima, New boronates prepared from 2,4-pentanedione derived ligands of the NO_2 and N_2O_2 type – comparison to the complexes obtained from the corresponding salicylaldehyde derivatives, J. Organomet. Chem. 689 (2004) 811-822 https://doi.org/10.1016/j.jorganchem.2003.11.032.
[27] A.D. Khalaji, A.N. Chermahini, K. Fejfarova, M. Dusek, Synthesis, characterization, crystal structure, and theoretical studies on Schiff-base compound 6-[(5-Bromopyridin-2-yl)iminomethyl]phenol, Struct. Chem. 21 (2010) 153-157 https://doi.org/10.1007/s11224-009-9554-5.
[28] G. Pavlovic, J.M. Sosa, D. Vikic-Topic, I. Leban, N-(3-Chlorophenyl)-2-hydroxy-1-naphthaldimine at 200 K, Acta. Crystallogr. E Acta. Cryst. E 58 (2002) o317-o320 https://doi.org/10.1107/S1600536802003057.
[29] F.H. Allen, O. Kennard, D.G. Watson, L. Brammer, A.G. Orpen, Prekin trans 2, Tables of bond lengths determined by *X*-ray and neutron diffraction. Part 1. Bond lengths in organic compounds, J. Chem. Soc. (1987) S1-S19.
[30] Z. Hu, Q. Deng, Z. Jiang, Z. Guo, D. Guo, "AIE+ESIPT" bis Schiff-base ligands with multicolor emission and their corresponding Eu(III) complexes: Synthesis and properties research, J. Lumin. (2020) 116929 https://doi.org/10.1016/j.jlumin.2019.116929.
[31] H.M. Abd El-Lateef, A.M. Abu-Dief, M.A. A. Mohamed, Corrosion inhibition of carbon steel pipelines by some novel Schiff base during acidizing treatment of oil wells studied by electrochemical and quantum chemical methods, J. Mol. Struct. 1130 (2017) 522-542 https://doi.org/10.1016/j.molstruc.2016.10.078.
[32] E.E. Elemike, H.U. Nwankwo, D.C. Onwudiwe, E.C. Hosten, Synthesis, structures, spectral properties and DFT quantum chemical calculations of (E)-4-(((4-propylphenyl)imino)methyl)phenol and (E)-4-((2-tolylimino)methyl)phenol; their corrosion inhibition studies of mild steel in aqueous HCl, J. Mol. Struct. 1141 (2017) 12-22 https://doi.org/10.1016/j.molstruc.2017.03.071.
[33] R.M. Issa, A.M. Khedr, H. Rizk, 1H NMR, IR and UV/VIS Spectroscopic Studies of Some Schiff Bases Derived From 2-Aminobenzothiazole and 2-Amino-3-hydroxypyridine, J. Chin. Chem. Soc. 55 (2008) 875-884 https://doi.org/10.1002/jccs.200800131.
[34] A.S. Alturiqi, A.M.A. Alaghaz, M.E. Zayed, R.A. Ammar, Synthesis, characterization, biological activity, and corrosion inhibition in acid medium of unsymmetrical tetradentate N2O2 Schiff base complexes, J. Chin. Chem. Soc. (2018) 1-15 https://doi.org/10.1002/jccs.201800027.
[35] H.M. Abd El-Lateef, Corrosion inhibition characteristics of a novelsalycilidene isatin hydrazine sodium sulfonate on carbon steel in HCl and a synergistic nickel ions additive: a combined experimental and theoretical perspective, Appl. Surf. Sci. 501 (2020) 144237 https://doi.org/10.1016/j.apsusc.2019.144237.

[36]M. Sarıgül, S.E. Kariper, P. Deveci, H. Atabey, D. Karakaş, M. Kurtoglu, Multi-properties of a new azo-Schiff base and its binuclear copper (II) chelate: Preparation, spectral characterization, electrochemical, potentiometric and modelling studies, J. Mol. Struct. 1149 (2017) 520-529 https://doi.org/10.1016/j.molstruc.2017.08.016.
[37] S. Nabatipour, S. Mohammadi, A. Mohammadi, Synthesis and comparison of two chromone based Schiff bases containing methoxy and acetamido substitutes as highly sustainable corrosion inhibitors for steel in hydrochloric acid, J. Mol. Struct. 1217 (2020) 128367 https://doi.org/10.1016/j.molstruc.2020.128367.
[38] M.A. Bedair, M.M.B. El-Sabbah, A.S. Fouda, H.M. Elaryian, Synthesis, electrochemical and quantum chemical studies of some prepared surfactants based on azodye and Schiff base as corrosion inhibitors for steel in acid medium, Corrosion Sci. 128 (2017) 54e72 https://doi.org/10.1016/j.corsci.2017.09.016.
[39] H. Ashassi-Sorkhabi, B. Shaabani, D. Seifzadeh, Corrosion inhibition of mild steel by some schiff base compounds in hydrochloric acid, Appl. Surf. Sci. 239 (2005) 154-164 **https://doi.org/10.1016/j.apsusc.2004.05.143.**
[40] J. Aljourani, K. Raeissi, M.A. Golozar, Benzimidazole and its derivatives as corrosion inhibitors for mild steel in 1M HCl solution, Corros. Sci. 51 (2009) 1836-1843 https://doi.org/10.1016/j.corsci.2009.05.011.
[41] K.C. Emregül and O. Atakol, Corrosion inhibition of iron in 1 M HCl solution with Schiff base compounds and derivatives, Mater. Chem. Phys. 83 (2004) 373-379. https://doi.org/10.1016/j.matchemphys.2003.11.008.
[42] I.L. Rosenfield, Corrosion Inhibitors, McGraw-Hil, New York, (1981) p.301.
[43] M.A. Hegazy, A novel Schiff base-based cationic gemini surfactants: Synthesis and effect on corrosion inhibition of carbon steel in hydrochloric acid solution, Corros. Sci. 51 (2009) 2610-2618 https://doi.org/10.1016/j.corsci.2009.06.046.
[44] N. Zulfareen, K. Kannan, T. Venugopal, S. Gnanavel, Synthesis, Characterization and Corrosion inhibition efficiency of N-(4-(Morpholinomethyl carbamoyl phenyl) Furan-2-Carboxamide for Brass in HCl Medium, Arab. J. Chem. 9 (1) (2016) 121-135 http://dx.doi.org/10.1016/j.arabjc.2015.08.023.
[45] H. Derya Leçe, K.C. Emregül, O. Atakol, Difference in the inhibitive effect of some Schiff base compounds containing oxygen, nitrogen and sulfur donors, Corros. Sci. 50 (2008) 1460-1468 https://doi.org/10.1016/j.corsci.2008.01.014.
[46] X. Li, S. Deng, H. Fu, Synergism between red tetrazolium and uracil on the corrosion of cold rolled steel in H_2SO_4 solution, Corros. Sci. 51(6) (2009) 1344-1355. https://doi.org/10.1016/j.corsci.2009.03.023.
[47] K. Zhang, W. Yang, B. Xu, X. Yin, Y. Chen, Y. Liu, Green Synthesis of Novel Schiff Bases as Eco-friendly Corrosion Inhibitors for Mild Steel in Hydrochloric Acid, ChemistrySelect. 3 (2018) 12486-12494 https://doi.org/10.1002/slct.201802915.
[48] M. Behpour, S.M. Ghoreishi, N. Soltani, M. Salavati-Niasari, The inhibitive effect of some bis-N,S-bidentate Schiff bases on corrosion behaviour of 304 stainless steel in hydrochloric acid solution, Corros. Sci. 51 (2009) 1073-1082. https://doi:10.1016/j.corsci.2009.02.011.
[49] S.M. Shaban, A. Saied, S.M. Tawfik, A. Abd-Elaal, I. Aiad, Corrosion inhibition and Biocidal effect of some cationic surfactants based on Schiff base, J. Ind. Eng. Chem. 19 (2013) 2004-2009 http://dx.doi.org/10.1016/j.jiec.2013.03.013.
[50] L. Li, Q. Qu, W. Bai, F. Yang, Y. Chen, S. Zhang, Z. Ding, Sodium Diethyldithiocarbamate as a Corrosion Inhibitor of Cold Rolled Steel in 0.5 M Hydrochloric Acid Solution, Corros. Sci. 59 (2012) 249-257 https://doi.org/10.1016/j.corsci.2012.03.008.

[51] O. Benali, L. Larabi, Y. Harek, Adsorption and Inhibitive Corrosion Properties of Thiourea Derivatives on Cold Rolled Steel in 1 M $HClO_4$ Solutions, J. Appl. Electrochem. 39 (2009) 769-778 https://doi.org/10.1007/s10800-008-9717-x.
[52] A. Boutouil, I. Elazhary, M.R. Laamari, H. Ben El Ayouchia, H. Anane, M. El Haddad, S.E. Stiriba, An exploration of corrosion inhibition of mild steel in sulphuric acid solution through experimental study and Monte Carlo simulations, J. Adhes. Sci. Technol. 34 (2020) 549-578 https://doi.org/10.1080/01694243.2019.1681741.
[53] Y. Ji, B. Xu, W. Gong, X. Zhang, X.g Jin, W. Ning, Y. Meng, W. Yang, Y. Chen, Corrosion inhibition of a new Schiff base derivative with two pyridine rings on Q235 mild steel in 1.0 M HCl, J. Taiwan. Inst. Chem. Eng. 000 (2016) 1-12 http://dx.doi.org/10.1016/j.jtice.2016.07.007.
[54] G. Khan, W.J. Basirun, S.N. Kazi, P. Ahmed, L. Magaji, S.M. Ahmed, G.M. Khan, M.A. Rehman, Electrochemical investigation on the corrosion inhibition of mild steel by Quinazoline Schiff base compounds in hydrochloric acid solution, J. Colloid. Interface. Sci. 502 (2017) 134-145 http://dx.doi.org/10.1016/j.jcis.2017.04.061.
[55] C. Loganayagi, C. Kamal, M.G. Sethuraman, Opuntiol: An Active Principle of Opuntia elatior as an Eco-Friendly Inhibitor of Corrosion of Mild Steel in Acid Medium, ACS Sustainable Chem. Eng. 2 (2014) 606-613 https://doi.org/10.1021/sc4003642.
[56] Y. Ma, F. Han, Z. Li, C. Xia, Acidic-Functionalized Ionic Liquid as Corrosion Inhibitor for 304 Stainless Steel in Aqueous Sulfuric Acid, ACS Sustainable Chem. Eng. 4 (9) (2016) 5046-5052 https://doi.org/10.1021/acssuschemeng.6b01492.
[57] M. Dahmani, A. Et-Touhami, S.S. Al-Deyab, B. Hammouti, A. Bouyanzer, Corrosion Inhibition of C38 Steel in 1 M HCl: A Comparative Study of Black Pepper Extract and Its Isolated Piperine, Int. J. Electrochem. Sci. 5 (2010) 1060-1069 http://www.electrochemsci.org/papers/vol5/5081060.pdf.
[58] X. Li, S. Deng, T. Lin, X. Xie, G. Du, 2-Mercaptopyrimidine as an effective inhibitor for the corrosion of cold rolled steel in HNO3 solution, Corros. Sci. 118 (2017) 202-216 http://dx.doi.org/doi:10.1016/j.corsci.2017.02.011.
[59] H. Heydari, M. Talebian, Z. Salarvand, K. Raeissi, M. Bagheri, M.A. Golozar, Comparison of two Schiff bases containing O-methyl and nitro substitutes for corrosion inhibiting of mild steel in 1 M HCl solution, J. Mol. Liq. 254 (2018) 177-187 https://doi.org/10.1016/j.molliq.2018.01.112.
[60] R. Kooliyat, J.T. Kakkassery, V.P. Raphael, **S.V. Cheruvathur, B.M. Paulson**, Synthesis, Cyclic Voltammetric, Electrochemical, and Gravimetric Corrosion Inhibition Investigations of Schiff Base Derived from 5, 5-Dimethyl-1, 3-cyclohexanedione and 2-Aminophenol on mild steel in 1 M HCl and 0.5 M H_2SO_4, Int. j. electrochem. 2019 (2019) 1-13 https://doi.org/10.1155/2019/1094148.
[61] D.K. Verma, A. Al Fantazi, C. Verma, F. Khan, A. Asatkar, C.M. Hussain, E.E. Ebenso, Experimental and computational studies on hydroxamic acids asenvironmental friendly chelating corrosion inhibitors for mildsteel in aqueous acidic medium, J. Mol. Liq. 314 (2020) 113651 https://doi.org/10.1016/j.molliq.2020.113651.
[62] M. Murmu, S.K. Saha, N.C. Murmu, P. Banerjee, Effect of stereochemical conformation into the corrosion inhibitive behaviour of double azomethine based Schiff bases on mild steel surface in 1 mol L^{-1} HCl medium: An experimental, density functional theory and molecular dynamics simulation study, Corros. Sci. 146 (2019) 134-151 https://doi.org/10.1016/j.corsci.2018.10.002.
[63] A. Espinoza-Vázquez, F.J. Rodríguez-Gómez, G.E. Negrón-Silva, R. González-Olvera, D. Ángeles-Beltrán, M. Palomar-Pardavé, A. Miralrio, M. Castro, Fluconazole and fragments as corrosion inhibitors of API 5L X52 steel immersed in 1M HCl, Corros. Sci. 174 (2020) 108853 https://doi.org/10.1016/j.corsci.2020.108853.

[64] Z. Rouifi, M. Rbaa, A.S. Abousalem, F. Benhiba, T. Laabaissi, H. Oudda, B. Lakhrissi, A. Guenbour, I. Warad, A. Zarrouk, Synthesis, characterization and corrosion inhibition potential of newly benzimidazole derivatives: Combining theoretical and experimental study, Surf. Interfaces. 18 (2020) 100442 https://doi.org/10.1016/j.surfin.2020.100442.
[65] O. Fergachi, F. Benhiba, M. Rbaa, M. Ouakki, M. Galai, R. Touir, B. Lakhrissi, H. Oudda, M. Ebn Touhami, Corrosion Inhibition of Ordinary Steel in 5.0 M HCl Medium by Benzimidazole Derivatives: Electrochemical, UV–Visible Spectrometry, and DFT Calculations, Journal of Bio- and Tribo-Corrosion 5(21) (2019) 1-13 https://doi.org/10.1007/s40735-018-0215-3.
[66] P. Dohare, M.A. Quraishi, I.B. Obot, A combined electrochemical and theoretical study of pyridine-based Schiff bases as novel corrosion inhibitors for mild steel in hydrochloric acid medium, J. Chem. Sci. 130(8) (2018) 1-19 https://doi.org/10.1007/s12039-017-1408-x.
[67] S. Vikneshvaran, S. Velmathi, Schiff Bases of 2,5 Thiophenedicarboxaldehyde as Corrosion Inhibitor for Stainless Steel under Acidic Medium: Experimental, Quantum Chemical and Surface Studies, ChemistrySelect 4 (2019) 387-392. https://doi.org/10.1002/slct.201803235.
[68] E. Ermis, Synthesis, spectroscopic characterization and DFT calculations of novel Schiff base containing thiophene ring, J. Mol. Struct. 1156 (2018) 91-104. https://doi.org/10.1016/j.molstruc.2017.11.089.
[69] D.S. Zinad, M. Hanoon, R.D. Salim, S.I. Ibrahim, A.A. Al-Amiery, M.S. Takriff, A.A.H. Kadhum, A new synthesized coumarin-derived Schiff base as a corrosion inhibitor of mild steel surface in HCl medium: gravimetric and DFT studies, Int. J. Corros. Scale Inhib. 9 (1) (2020) 228-243 https://doi.org/10.17675/2305-6894-2020-9-1-14.
[70] N.O. Obi-Egbedi , K.E. Essien, I.B. Obot, E.E. Ebenso, 1,2-Diaminoanthraquinone as Corrosion Inhibitor for Mild Steel in Hydrochloric Acid: Weight Loss and Quantum Chemical Study, Int. J. Electrochem. Sci. 6 (2011) 913-930.
[71] L. Toukal, S Keraghel, F. Benghanem, A. Ourari, Electrochemical, Thermodynamic and Quantum Chemical Studies of Synthesized Benzimidazole Derivative as an Eco-Friendly Corrosion Inhibitor for XC52 Steel in Hydrochloric Acid, *Int. J. Electrochem. Sci.*, 13 **(2018)** 951-974 https://doi.org/10.20964/2018.01.43.
[72] A. Singh, K.R. Ansari, M. Quraishi, H. Lgaz, Effect of Electron Donating Functional Groups on Corrosion Inhibition of J55 Steel in a Sweet Corrosive Environment: Experimental, Density Functional Theory, and Molecular Dynamic Simulation, Materials 12 (17) (2019) 17 https://doi.org/10.3390/ma12010017.
[73] X. Si-Wei, L. Zheng, H. Guo-Cheng, L. Wei, L. Jin , C. Zhen Cheng, Molecular dynamics simulation of inhibition mechanism of 3,5-dibromo salicylaldehyde Schiff's base, Comput. Theor. Chem. 1063 (2015) 50-62 https://doi.org/10.1016/j.comptc.2015.04.003.